AFCRL-64-608

THE REFRACTED ARRIVAL FROM A LAYER

T. W. Spencer

California Research Corporation

La Habra, California

Contract No. AF19(604)-8344

Scientific Report Number 6

June 15, 1964

Project 8652

Task 865205

Prepared for

AIR FORCE CAMBRIDGE RESEARCH LABORATORIES
OFFICE OF AEROSPACE RESEARCH
UNITED STATES AIR FORCE
BEDFORD, MASSACHUSETTS

WORK SPONSORED BY ADVANCED RESEARCH PROJECTS AGENCY

PROJECT VELA-UNIFORM

ARPA Order No. 180-61
Project Code No. 8100 Task 2

Request for additional copies by Agencies of the Department of Defense, their contractors, and other government agencies should be directed to the:

DEFENSE DOCUMENTATION CENTER (DDC)
CAMERON STATION
ALEXANDRIA, VIRGINIA

Department of Defense Contractors must be established for DDC services or have their "need-to-know" certified by the cognizant military agency of their project or contract.

All other persons and organizations should apply to the:

U. S. DEPARTMENT OF COMMERCE
OFFICE OF TECHNICAL SERVICES
WASHINGTON, D. C. 20230

THE REFRACTED ARRIVAL FROM A LAYER

T. W. Spencer

ABSTRACT

High-frequency geometric ray theory is used to investigate the refracted arrival from a high-speed layer embedded in an infinite medium. The effect of changing the layer thickness to dominant wavelength ratio (E/λ_d) and the range to depth ratio (ρ/H) is analyzed for a point compressional source. The results approximate the exact solution when $E/\lambda_d \geq 1$. The theory predicts shingling and shows that it is distance-limited. The maximum distance at which shingling is observed decreases as E/λ_d decreases. Beyond a certain minimum distance, the refracted arrival consists of a superposition of waves whose phase velocities approach the compressional velocity in the layer at large distances. These waves include the reflected waves which cross the layer at least once in the compressional mode and the head waves which are generated by reflected waves which do not cross the layer in the compressional mode. There are

$$D_{nm} = (n+m)!/n!m!$$

reflected ray paths which cross the layer n times in the compressional mode and m times in the shear mode which arrive at exactly the same time. A formula is derived which expresses the composite amplitude of these rays in the form of a series which

contains either m or $n+1$ terms (whichever is smaller). The travel-time curves for all rays with the same m value approach the same asymptote regardless of the n values. At large distances the travel-time curves for waves whose m values differ by one approach asymptotes which differ by T_Δ . At large distances and for thin layers, the total amplitude obtained by summing all rays with the same m value satisfies

$$A_m \sim \gamma_m (\rho/H)^{-3/2} (E/H)^{1/2} .$$

The γ_m depend only on the density and velocity ratios. Because the head waves decay like $(\rho/H)^{-2}$, the reflected waves predominate at large distances. If the duration of the direct wave is less than T_Δ , the refracted arrival consists of a series of events - each associated with a different m value. At large distances, the onsets of the events are separated by T_Δ , the amplitudes decay like $(\rho/H)^{-3/2}$ and the γ_m determine the relative amplitudes.

CONTENTS

INTRODUCTION

The refracted wave generated at the plane interface between two half spaces has been studied extensively by Heelan (1953), Strick (1959), Dix (1961) and Gilbert and Laster (1962). For studies of explosion-generated waves, the results for a point compressional source are of particular significance. High-frequency theory predicts that the refracted wave varies with time in a manner which is determined by the integral of the direct wave (measured at distances large compared with the wavelengths of interest) and the amplitude decays with distance like $\rho^{-1/2} L^{-3/2}$. ρ is the horizontal source-receiver separation and L is the distance traveled in the refractor. Donato (1964a) has determined the minimum range (in terms of the dominant wavelength) at which the high-frequency approximation is valid.

When the high-velocity medium is finite in thickness, the problem may be considerably more complicated. To demonstrate this, let T be the duration of the head wave for an infinitely thick layer and let t_r be the head wave travel time. The results for an infinitely thick layer are not valid if waves which are multiply reflected within the layer or other wave types arrive in the interval $t_r \leq t \leq t_r + T$. Multiple reflections distort the refracted arrival when T is large, the layer is thin or the offset is large. When any of these conditions are satisfied, the individual phases are not resolved and the character and amplitude of the refracted arrival are determined by the way in which the individual phases interfere with one another. Interference explains the amplitude dependence on offset and on the

dominant wavelength to thickness ratio, the discrepancy between the actual velocity in the layer and the measured velocity, the error in determining the true beginning of the arrival and the phenomenon of shingling[1].

Dunkin (1963) and Donato (1964b) have investigated theoretically the first extremum produced by the interference of the head wave and the compressional wave reflected off the bottom of the layer. Their theoretical predictions for the dependence of phase velocity on layer thickness and the dependence of amplitude on range are in general agreement with model experiments (Lavergne, 1961, and Levin and Ingram, 1962). Various lines of experimental evidence (e.g., shingling) indicate that in certain situations the first extremum may be so weak that it is not detected. In this paper high-frequency geometric ray theory is used to compute the complete refracted wave train.

---

[1]Shingling occurs when the phase velocity exceeds the group velocity. As the range increases, peaks and troughs move forward through the envelope which defines the refracted arrival. In this process, the amplitude of the first extremum decreases and it is eventually lost in the noise. At this offset, a later extremum is selected to define the time-distance curve. At each offset where an extremum is lost, there is a discontinuity in the time-distance curve and a new shingle is added corresponding to a later, larger amplitude extremum.

THE EMBEDDED LAYER

Consider the problem of determining the refracted arrival from a high-velocity layer embedded in an infinite medium. This model avoids the complications introduced by putting in a free surface. The significance of the geometric quantities is indicated in Figure 1. The top of the layer is at a depth H below the source and at a depth Z below the receiver. The radiation field is axially symmetric about the Z axis. The Z axis passes through the source and is normal to the interface. The plane Z = 0 coincides with the top of the layer. Our computations are made for a horizontal refractor so that Z = H. A dipping refractor can also be investigated by using

$$|Z-H| = \rho_h \sin\phi$$

to relate Z and H. Here the refractor dips at an angle ϕ with respect to the horizontal plane in which the source and receiver are located and ρ_h is the source-receiver separation in the horizontal plane. E is the layer thickness. V is the compressional velocity, v is the shear velocity and b is the density. Subscript 1 refers to the infinite medium and subscript 2 refers to the layer.

The critical angle for P_1P_2 (incident compressional, transmitted compressional) is θ_c and the critical angle for P_1S_2 (incident compressional, transmitted shear) is θ_s .

DEGENERACY

When we attempt to take into account all the waves which are multiply reflected within the layer, we immediately encounter the problem of degeneracy. The simplest case of degeneracy arises when the ray crosses the layer once in the compressional (P) mode and once in the shear (S) mode. In Figure 1 we see that there are two such rays which arrive at exactly the same time and are therefore degenerate. These two rays differ in the sequence in which the P and S legs of the path are traversed. This type of degeneracy cannot be removed by changing the layer thickness or velocity. It is a consequence of the fact that two different types of waves can propagate in an elastic medium. Degeneracy occurs only for rays which cross the layer in both modes.

To reduce this idea to quantitative terms, we introduce the following definitions:

n number of crossings in the P mode,

m number of crossings in the S mode.

Specifying n and m determines a family of degenerate rays. The number of rays in the family (i.e., the degeneracy) is given by

$$D_{nm} = (n+m)!/n!m! \qquad (1)$$

Even when $n = 6$ and $m = 2$, the degeneracy is 28. If highly degenerate events are truly significant, a way must be found for removing the degeneracy - otherwise the ray theory becomes extremely inefficient from a computational standpoint. Also, because all the degenerate rays arrive at the same time, only the composite event has physical significance. For the embedded layer, a simple technique exists for removing the degeneracy.

REMOVAL OF DEGENERACY

For illustrative purposes, we consider waves which leave the source and arrive at the detector in the compressional mode. The total amplitude of a degenerate event must be expressible in the form

$$A_{nm} = (T_{P_1P_2}T_{P_2P_1})Q_{nm} + (T_{P_1S_2}T_{S_2P_1})S_{nm} + (T_{P_1P_2}T_{S_2P_1})U_{nm} + (T_{P_1S_2}T_{S_2P_1})W_{nm} \qquad (2)$$

The T's are transmission coefficients. The letter subscripts indicate the mode of propagation before and after transmission. The numbers indicate the media in which the wave propagates. Q_{nm} gives the total amplitude of all waves which make the first and last crossing in the layer in the compressional mode. The significance of each quantity is indicated below:

Symbol	First Crossing	Last Crossing
Q_{nm}	P	P
S_{nm}	S	P
U_{nm}	P	S
W_{nm}	S	S

The transmission coefficients appear explicitly in (2). Q_{nm}, S_{nm}, U_{nm} and W_{nm} are functions of the reflection coefficients R_{PP}, R_{PS}, R_{SP} and R_{SS}. There are only four reflection coefficients because the wave can approach the interfaces only from within the layer and the external media have identical properties.

Formulas which give Q_{nm} , S_{nm} , U_{nm} and W_{nm} in terms of the reflection coefficients can be derived by using the procedure outlined below for Q_{nm} . Partition the m shear crossings into q groups. Each group must contain at least one shear crossing. q satisfies

$$1 \leq q \leq \text{minimum}(n-1, m) \quad , \quad m \geq 1, n \geq 2 .$$

The number of ways of distributing m identical things among q groups is

$$\beta_{m,q} = \frac{(m-1)!}{(m-q)!(q-1)!}$$

If there are q groups of S, there must be $q+1$ groups of P (since for Q_{nm} the first and last leg must be in the P mode). The number of ways of distributing the n compressional crossings into $q+1$ groups is $\beta_{n,q+1}$. Consequently, the total number of P-S sequences in which the S are arranged in q groups is $\beta_{m,q}\,\beta_{n,q+1}$.

The exponents for the reflection coefficients can be derived just as easily. There are q groups of S. This indicates that there are q conversions from P to S and from S back to P. R_{PS} and R_{SP} enter in the form

$$(R_{PS}R_{SP})^{q}$$

Let χ_i be the number of shear crossings in the i^{th} group. $\chi_i - 1$ is the number of SS reflections in the i^{th} group. The total number of SS reflections is

$$\sum_{i=1}^{q} (\chi_i - 1) = m - q .$$

$m-q$ is the exponent of R_{SS}. The total number of reflections is given by $n+m-1$. We have already accounted for $m-q+2q = m+q$ reflections. Therefore, the number of PP reflections is

$$(n+m-1)-(m+q) = n-q-1 .$$

The final expression for Q_{nm} is

$$Q_{nm} = \sum_{q=1}^{\min(n-1,m)} \beta_{m,q}\beta_{n,q+1}(R_{PS}R_{SP})^{q} R_{SS}^{m-q} R_{PP}^{n-q-1} , \quad m\geq 1,\ n\geq 2 .$$

The final expression for the total amplitude is

$$A_{nm} = \sum_{q=1}^{\min(m,n+1)} \beta_{m,q}(R_{PS}R_{SP})^{q-1} R_{SS}^{m-q} R_{PP}^{n-q+1} \left\{ \beta_{n,q+1} \frac{R_{PS}R_{SP}}{R_{PP}^{2}} T_{P_1P_2}T_{P_2P_1} + \frac{\beta_{n,q}}{R_{PP}} \left(R_{SP}T_{P_1S_2}T_{P_2P_1} + R_{PS}T_{P_1P_2}T_{S_2P_1} \right) + \beta_{n,q-1} T_{P_1S_2}T_{S_2S_2}T_{S_2P_1} \right\}, \quad m\geq 1, n\geq 1. \tag{3}$$

The total amplitude for the trivial cases where either n or m is zero is

$$A_{n,0} = R_{PP}^{n-1}\left(T_{P_1P_2}T_{P_2P_1}\right) ,$$
$$A_{0,m} = R_{SS}^{m-1}\left(T_{P_1S_2}T_{S_2P_1}\right). \tag{4}$$

Instead of computing the amplitudes of D_{nm} individual degenerate rays, we need evaluate only m or $n+1$ (whichever is smaller) terms in a series. It is this fact which permits the rapid computation of highly degenerate events. Furthermore, the use of (3) avoids the complicated bookkeeping required to insure that all members of the degenerate family have been included.

In the derivation we confined our attention to a geometrical situation in which the source and receiver were on the same side of the layer and to rays which leave the source and arrive at the detector in the P mode. The same method yields the total amplitude when the waves leave the source and arrive at the detector in either the P or S mode and

(a) the source is in the half-space and the receiver is in the layer (or vice versa),

(b) the source and receiver are on opposite sides of the layer,

(c) the source and receiver are in the layer.

HIGH-FREQUENCY THEORY

Knowing A_{nm} we can derive information about the refracted arrival by using the method of generalized reflection and transmission coefficients (Spencer, 1960). To use this method, we require an integral representation for the Laplace transform of the source radiation field. The vertical component of particle velocity in a spherically symmetric compressional wave is

$$U_o = -\left(\frac{P_o a}{b_1}\right)\frac{1}{rV_1}\left(\frac{z-H}{r}\right)\left\{\gamma(\tau) + \frac{t_d V_1}{r}\int_0^{\tau}\gamma(\xi)\,d\xi\right\},$$
$$\tau = \frac{t - r/V_1}{t_d} \qquad r = \left\{\rho^2 + (z-H)^2\right\}^{1/2}. \tag{5}$$

The source function, γ, is time-limited and merely expands or contracts with t_d but does not change shape. The amplitude spectrum of γ is assumed to peak at a dominant frequency $f_d = 1/t_d$. r is the distance between source and receiver. At distances which are large compared with the dominant wavelength, the direct wave propagates without change of shape and the time variation is given by $\gamma(\tau)$. a is the radius of the spherical cavity and P_o is the peak pressure applied to the cavity wall.

The Laplace transform of (5) is

$$\bar{U}_o = -\left(\frac{P_o a}{b_1}\right)\bar{\gamma}\left(1 + \frac{V_1}{Sr}\right)\left(\frac{z-H}{r}\right)\frac{e^{-Sr/V_1}}{rV_1} = \left(\frac{P_o a}{b_1}\right)(\operatorname{sign}(z-H))\frac{\bar{\gamma}}{S}\int_0^{\infty}\lambda J_o(\lambda\rho)e^{-\alpha_1|z-H|}\,d\lambda,$$

$$\alpha_1 = \left(\lambda^2 + \frac{S^2}{V_1^2}\right)^{1/2}.$$

Using the method of generalized coefficients gives the Laplace transform of the composite event specified in equation (3) as

$$\bar{U}_{n,m} = -\left(\frac{P_0 a}{b_1}\right)\frac{\bar{X}}{S}\int_0^\infty \lambda J_0(\lambda\rho) A_{nm}(\lambda,S) e^{-K_{nm}(\lambda,S)}\, d\lambda \,, \tag{6}$$

where

$$K_{nm} = (H+Z)\left(\lambda^2+\frac{S^2}{V_1^2}\right)^{1/2} + nE\left(\lambda^2+\frac{S^2}{V_2^2}\right)^{1/2} + mE\left(\lambda^2+\frac{S^2}{V_2^2}\right)^{1/2}.$$

Cagniard's method (1961) gives the response function corresponding to $\bar{U}_{nm}$ in terms of a contour integral. The numerical integration is time consuming even on a computer in the IBM 7094 class. For a line source, the Bessel function in (6) is replaced by the exponential $e^{i\lambda y}$ (the line source coincides with the x axis). Garvin (1956), by applying Cagniard's method to the line-source problem, obtained a closed algebraic expression for the response. This function can be evaluated rapidly on the IBM 7094. The total solution for our problem is built up by superposing the response functions for all rays which arrive during the time interval of interest. If there are a great many rays, the computation of the total response is time consuming even though the computation time per ray is nominal. Because of this and other difficulties, we have derived an approximation to the exact response function which is valid in some high-frequency limit. The low-frequency cutoff will become apparent later when we plot the amplitude of the refracted arrival against the dominant wavelength to thickness ratio.

The high-frequency asymptotic expansion of (6) can be obtained by using the method of steepest descent and a modification of the method of stationary phase discussed by Erdelyi (1956). The asymptotic representation for the composite reflection is designated by a superscript r and is

$$\left(\frac{H}{a}\right)^{3/2}\frac{b_1 V_1}{P_0}U^r_{nm} = R^r_{nm}\left(\frac{t}{H/V_1}, \frac{t_d}{H/V_1}, \frac{\rho}{H}, \frac{E}{H}, \frac{Z}{H}\right)$$

$$-\frac{G_{nm}}{\left(\frac{t_d}{H/V_1}\right)^{1/2}}\left\{\frac{\mathcal{I}A_{nm}(-i\sin\theta_{nm})}{\pi}\int_{(t-T)/(H/V_1)}^{t/(H/V_1)}\chi\left(\frac{\frac{t}{H/V_1}-T}{\frac{t_d}{H/V_1}}\right)\frac{dT}{T-T_{nm}} - \mathcal{R}A_{nm}(-i\sin\theta_{nm})\chi\left(\frac{\frac{t}{H/V_1}-T_{nm}}{\frac{t_d}{H/V_1}}\right)\right\}, \quad (7)$$

where $\mathcal{I}A_{nm}$ refers to the imaginary part of A_{nm} and $\mathcal{R}A_{nm}$ to the real part. Arons and Yennie (1950) derived a similar result by considering the reflection of a plane wave from a liquid-solid interface. Equation (7) shows that their result remains valid for a multiply reflected wave which is initially spherical in shape. θ_{nm} is the angle of incidence at the upper interface of the rays which cross the layer n times in the compressional mode and m times in the shear mode. $A_{nm}(-i\sin\theta_{nm})$ is a function of the plane wave reflection and transmission coefficients. Inside the critical angle ($\theta_{nm} < \theta_c$), $A_{nm}(-i\sin\theta_{nm})$ is pure real, the first term in (7) vanishes and the time variation in the reflected wave is determined by the source function. Each reflected wave propagates with a phase velocity which depends on the range. Waves which cross the layer at least once in the compressional

mode ($n \geq 1$) propagate with phase velocities which approach the compressional velocity in the layer at large distances. All other reflected waves have phase velocities which approach either the compressional velocity in the half space or the shear velocity in the layer. Therefore, beyond a certain minimum distance (which depends on the time interval of interest) only reflected waves which satisfy the condition $n \geq 1$ can contribute to the refracted arrival. For these waves the angle of incidence is less than the critical angle and the wave shape is determined by the source function.

G_{nm} takes into account the diminution in amplitude produced by geometric spreading

$$G_{nm} = \left[\left(\frac{\sin\theta_{nm}}{\rho/H} \right) \Big/ \left\{ \frac{1+\frac{Z}{H}}{(1-\sin^2\theta_{nm})^{3/2}} + \frac{n\frac{E}{H}\frac{V_1^2}{V_2^2}}{\left(\frac{V_1^2}{V_2^2}-\sin^2\theta_{nm}\right)^{3/2}} + \frac{m\frac{E}{H}\frac{V_1^2}{V_2^2}}{\left(\frac{V_1^2}{V_2^2}-\sin^2\theta_{nm}\right)^{3/2}} \right\} \right]^{1/2}.$$

$\sin\theta_{nm}$ is an implicit function of the geometric parameters through the relation

$$\frac{\rho}{H} = \sin\theta_{nm} \left\{ \frac{1+\frac{E}{H}}{(1-\sin^2\theta_{nm})^{1/2}} + \frac{n\frac{E}{H}}{\left(\frac{V_1^2}{V_2^2}-\sin^2\theta_{nm}\right)^{1/2}} + \frac{m\frac{E}{H}}{\left(\frac{V_1^2}{V_2^2}-\sin^2\theta_{nm}\right)^{1/2}} \right\}$$

and τ_{nm} is the normalized travel time

$$\tau_{nm} = \frac{t_{nm}}{H/V_1} = \frac{1+\frac{Z}{H}}{(1-\sin^2\theta_{nm})^{1/2}} + \frac{n\frac{E}{H}\frac{V_1^2}{V_2^2}}{\left(\frac{V_1^2}{V_2^2}-\sin^2\theta_{nm}\right)^{1/2}} + \frac{m\frac{E}{H}\frac{V_1^2}{V_2^2}}{\left(\frac{V_1^2}{V_2^2}-\sin^2\theta_{nm}\right)^{1/2}}.$$

These relations show that except for the factor $(H/a)^{3/2} b_1 V_1 / P_o$, the response expressed as a function of $t/(H/V_1)$ depends on the three geometric parameters ρ/H, E/H and Z/H and on the dominant wavelength to thickness ratio through the parameter

$$\frac{t_d}{H/V_1} = \frac{\lambda_d}{H} = \left(\frac{\lambda_d}{E}\right)\frac{E}{H} .$$

The reflected waves which do not cross the layer in the compressional mode ($\eta = 0$) generate head waves. The head waves which propagate with a phase velocity V_2 are components of the refracted arrival. The wave reflected from the top of the layer generates the ordinary head wave indicated by the segment ED in the upper diagram in Figure 2. This wave travels in the direction normal to ED with a velocity V_1 and has a constant phase velocity, V_2. The incident wave produces both a transmitted compressional wave ($P_1 P_2$) and a transmitted shear wave ($P_1 S_2$) in the layer. These two wavefronts intersect at the interface as long as the phase velocity in the incident wave exceeds V_2. When the phase velocity in the incident wave drops below V_2, the wavefronts separate. In this process an internal head wave is generated (BD). This wave travels in the direction normal to BD with a velocity v_2.

The lower diagram shows what happens when the transmitted shear wave and the head wave reflect off the bottom of the layer. BQ is the reflected part of the head wave. The incident shear wave (PC) generates a reflected compressional wave (QF) and a

reflected shear wave (PBA). At a point on the lower interface where the phase velocity of the incident shear wave drops below V_2, these two wavefronts begin to separate. A new head wave is generated whose wavefront coincides with BQ. Each time the unconverted shear wave ($\eta = 0$) is reflected back into the layer, a new head wave is generated whose wavefront coincides with the wavefront of head waves generated by earlier shear reflections.

The high-frequency representation for head waves which propagate with a phase velocity V_2 is

$$\left(\frac{H}{a}\right)^{3/2} \frac{b_1 V_1}{P_0} U_m^f = R_m^f\left(\frac{t}{H/V_1}, \frac{t_d}{H/V_1}, \frac{\rho}{H}, \frac{E}{H}, \frac{Z}{H}\right)$$
$$= \left(\frac{t_d}{H/V_1}\right)^{1/2} \frac{\mu_m}{\left(\frac{\rho}{H}\right)^2 \left(1-\frac{\rho_m}{\rho}\right)^{3/2}} \chi_I\left(\frac{\frac{t}{H/V_1} - \tau_m}{\frac{t_d}{H/V_1}}\right) \quad (m = 0, 2, 4, \ldots) \tag{8}$$

where

$$\chi_I(T) = \int_0^T \chi(\xi)\, d\xi \, .$$

and μ_m, ρ_m and τ_m are defined subsequently. The time variation is determined by the integral of the source function. At large offsets the amplitude decays like $(\rho/H)^{-2}$. The wavefront of the head wave is tangent to the reflected wave which generates it at the critical distance

$$\frac{\rho_m}{H} = \frac{V_1}{V_2}\left\{\frac{1+\frac{Z}{H}}{\left(1-\frac{V_1^2}{V_2^2}\right)^{1/2}} + \frac{m\frac{E}{H}}{\left(\frac{V_1^2}{2V_2^2} - \frac{V_1^2}{V_2^2}\right)^{1/2}}\right\}$$

and the normalized travel time is

$$\tau_m = \frac{t_m}{H/V_1} = \frac{\rho V_1}{H V_2} + \left(1+\frac{Z}{H}\right)\left(1-\frac{V_1^2}{V_2^2}\right)^{1/2} + m\frac{E}{H}\left(\frac{V_1^2}{2V_2^2} - \frac{V_1^2}{V_2^2}\right)^{1/2}.$$

The head waves are separated by equal time intervals

$$\frac{2T_\Delta}{H/V_1} = \frac{t_{m+2}-t_m}{H/V_1} = 2\frac{E}{H}\left(\frac{V_1^2}{2V_2^2}-\frac{V_1^2}{V_2^2}\right)^{1/2} \qquad (9)$$

which do not depend on the offset. This fact suggests that if the refracted arrival consisted of head waves alone, the condition $t_d = 2T_\Delta$ would lead to constructive interference when the μ_m all have the same polarity.

The μ_m depend on the velocity and density ratios and are defined by

$$\mu_m = \frac{1}{2}\frac{V_1}{V_2} i \left(\frac{dq_m}{d\chi}\right)_{\chi=0} , \quad \chi = \left(\xi^2 - \frac{V_1^2}{V_2^2}\right)^{1/2}, \qquad (10)$$

where

$$q_m(\xi) = f(\xi) - f^*(\xi).$$

$f^*(\xi)$ is the complex conjugate of $f(\xi)$. ξ may be identified with the sine of the angle of incidence. The form of $f(\xi)$ depends on the value of m as follows:

$$f(\xi) = R_{P_1P_1}(\xi) , \quad m=0 ;$$

$$f(\xi) = \left(T_{P_1S_2}(\xi)T_{S_2P_1}(\xi)\right) R_{S_2S_2}^{m-1}(\xi) , \quad m=2,4,\ldots.$$

$f(\xi)$ contains square roots of the form $(\xi^2 - f_i^2)^{1/2}$. A one-to-one correspondence between points in the ξ and $f(\xi)$ planes is established by introducing cuts of finite length along the real ξ-axis between each pair of branch points. Each square root is defined to be positve real on the real ξ-axis to the right of the cut. At large offsets the μ_m determine the relative strengths of the head waves.

The refracted arrival from the layer is composed of head waves and multiply reflected waves which cross the layer at least once in the compressional mode. All these waves propagate with a phase velocity which at large offsets approaches the compressional velocity in the layer. The reflected waves have the same shape as the source function. The shape of the head waves is determined by the time integral of the source function. To explain the significance of the factor $(t_d/(H/V_1))^{1/2}$ which appears in (7) and (8), we must re-examine the expression for the direct wave in (5). The total energy radiated into the system is

$$E_T \sim \left(\frac{P_0 a}{b_1}\right)^2 \frac{4\pi b_1}{V_1} t_d \int_0^{T/t_d} \chi^2(\xi)\, d\xi .$$

T is the duration of the source function (χ) and, for the form of source function we are assuming, T/t_d is a constant. The total energy input is directly proportional to t_d. We make the energy input independent of the dominant period by dividing the source function by the dimensionless quantity $(t_d/(a/V_1))^{1/2}$ The quantity $(t_d/(H/V_1))^{1/2}$ appears in the numerator in (8) because the shape of the head wave is determined by the integral of the source function and integration introduces a factor t_d. Note that in the high-frequency limit, the reflected waves determine the amplitude and character of the refracted arrival.

The complete expression for the refracted arrival is

$$\left(\frac{H}{a}\right)^{3/2}\frac{b_1 V_1}{P_o}U = R_Z\left(\frac{t}{H/V_1}, \frac{t_d}{H/V_1}, \frac{\rho}{H}, \frac{E}{H}, \frac{Z}{H}\right) = \tag{11}$$

$$-\frac{1}{\left(\frac{t_d}{H/V_1}\right)^{1/2}}\sum_{m=0}\sum_{n=1} G_{nm} A_{nm}(-i\sin\theta_{nm})\, \chi\left(\frac{\frac{t}{H/V_1}-\tau_{nm}}{\frac{t_d}{H/V_1}}\right) + \frac{\left(\frac{t_d}{H/V_1}\right)^{1/2}}{\left(\frac{\rho}{H}\right)^2}\sum_{(m=0,2,\cdots)} \frac{\mu_m}{\left(1-\frac{\rho_m}{\rho}\right)^{3/2}}\, \chi_I\left(\frac{\frac{t}{H/V_1}-\tau_m}{\frac{t_d}{H/V_1}}\right),$$

$$t < t_{co}.$$

When $V_1 > v_2$, t_{co} is the travel time of the first reflected arrival which is incident beyond the critical angle - this is the reflected wave $P_1 P_1$. When $V_1 < v_2$, a shear head wave is generated which propagates with the phase velocity v_2. Beyond the shear critical angle, θ_s, t_{co} is determined by the travel time of the shear head wave -

$$t_s = \frac{H}{V_1}\left\{\frac{V_1}{v_2}\frac{\rho}{H} + \left(1+\frac{Z}{H}\right)\left(1-\frac{V_1^2}{v_2^2}\right)^{1/2}\right\}.$$

Inside the shear critical angle, t_{co} is determined by the travel time of the first reflected wave which is incident beyond the critical angle θ_c. Note that inside the critical angle θ_c, there are no head waves and if we remove the restriction on η (i.e., $\eta \geq 1$) equation (11) gives the complete reflected arrival from the embedded layer.

CHARACTERISTICS OF THE MULTIPLY REFLECTED WAVES

For high frequencies the multiply reflected waves determine the characteristics of the refracted arrival. The travel-time curves for $m = 0,1,2$ are plotted in Figure 3. The difference in travel time between the reflected wave and the refracted arrival is plotted on the ordinate. The offset is plotted on a logarithmic scale to emphasize the fact that all the travel-time curves for a particular m value approach the same asymptote at large offsets - the travel-time difference between any two waves which have the same m value goes to zero at large offsets regardless of the n values. The travel-time difference between waves which have different m values approaches a finite value at large offsets which is a multiple of T_Δ. T_Δ is defined in (9) where it is shown that $2T_\Delta$ is the time interval between head wave arrivals.

This clustering of the travel-time curves leads us to refer to waves with the same m value as a particular order. If the significant amplitudes in each order are confined to a limited range of n values and T (source duration) $< T_\Delta$, the refracted arrival at large offsets appears as a series of events (Berckhemmer and Oliver, 1955). Each event is associated with a particular m value and propagates with a phase velocity which is very close to the compressional velocity in the layer. The amplitude of each event is obtained by summing the amplitudes of all rays which have the same m value as follows:

$$A_m = -\sum_n G_{nm} A_{nm} (-i \sin\theta_{nm}) . \qquad (12)$$

A_m is plotted against the normalized offset in Figure 4. At large offsets, the slope approaches -3/2. In Figure 5, A_m is plotted against the normalized layer thickness. For thin layers the slope approaches 1/2. A study of many cases shows that for $\rho/H > 20$ and $E/H < .1$,

$$A_m = \gamma_m (\rho/H)^{-3/2} (E/H)^{1/2} . \qquad (13)$$

At large offsets the head wave contributions decay like $(\rho/H)^{-2}$. This means that the reflected waves determine the character of the refracted arrival at large offsets.

The γ_m and μ_m depend on the compressional velocity ratio, the Poisson's ratios (σ_1 and σ_2) and the density ratio. In Figure 6, the γ_m and μ_m are plotted against the compressional velocity ratio for a rigid layer ($\sigma_2 = .25$) embedded in a very weak medium ($\sigma_1 = .45$).[2] For large velocity contrasts, the γ_m ($m \geq 1$) approach and even exceed γ_0. γ_1 is within 10 per cent of γ_0 over a large part of the range. γ_1 goes through zero between .86 and .87. This fact indicates that in the first order ($m = 1$) the amplitudes of the individual waves change sign at least once. If the amplitudes of the head wave and reflected

---

[2]Note that the measurements of McDonal, et al. (1958) indicate that at a depth of 500 ft, the Poisson's ratio in Pierre Shale is about .42.

wave contributions to the refracted arrival were determined by μ_m and γ_m alone, the reflected waves would be of minor importance over most of the range. However, increasing either the offset or the dominant frequency reduces the head wave amplitude relative to the reflected wave No significance should be attached to the behavior of μ_m near $V_1/V_2 = 1$. This is a consequence of the fact that the high-frequency asymptotic representation for the head wave is not valid when the receiver is near the critical cone. As V_1/V_2 approaches unity, the critical cone approaches the receiver regardless of where the receiver is located. Note that μ_2 decreases relative to μ_0 as the velocity contrast increases and is always less than five per cent of μ_0.

In Figure 7, the γ_m and μ_m are plotted against V_2^2/v_2^2. This quantity determines the Poisson's ratio

$$\sigma_2 = \frac{\frac{1}{2}\frac{V_2^2}{v_2^2} - 1}{\frac{V_2^2}{v_2^2} - 1}.$$

The higher orders peak sharply near $V_2^2/v_2^2 = 3.0 (\sigma_2 = .25)$. Near $V_2^2/v_2^2 = 3.0$, γ_2 is about 10 per cent of γ_0. As the layer becomes more fluid-like, the γ_m $(m \geq 1)$ decrease and become very small compared with γ_0. This is because the γ_m $(m \geq 1)$ depend on the conversion coefficients R_{PS} and R_{SP}. As the layer becomes more fluid-like, the efficiency of the compressional to shear conversion decreases. Similar behavior is exhibited by the μ_m.

In Figure 8 the γ_m and μ_m are plotted against V_1^2 / v_1^2. Over the entire range the γ_m ($m \geq 2$) are small compared with γ_o but as the infinite medium becomes more fluid-like, γ_1' approaches γ_o and even exceeds it. The μ_m ($m \geq 2$) have much larger values when the infinite medium is fluid-like than when it is rigid but only μ_2 ever exceeds 10 per cent of μ_o. Note that for large values of V_1^2 / v_1^2, all the higher orders have opposite polarity to μ_o.

Equation (12) cannot be used when the individual wavelets (corresponding to the different n values) are wholly or partially resolved. The degree of resolution increases as the offset decreases, the layer gets thicker or the dominant frequency increases. In Figure 9, the amplitude of each wave is plotted along the ordinate and the difference between the arrival time of the reflected wave and the onset of the refracted arrival along the abscissa. Here we consider only multiples which do not cross the layer in the shear mode ($m = 0$). Each curve is drawn for a particular offset. The leftmost dot on each curve gives the amplitude and time difference for the wave which crosses the layer twice in the compressional mode ($n = 2$). As we move along each curve from left to right, n increases in increments of two.

Note that the time interval between the arrival of events corresponding to different m values is .106. At each offset, all the significant amplitudes occur well within this

interval. It follows that if the first event is resolved at $\rho/H = 5$, it is resolved at all larger offsets.

The open dot on each curve corresponds to $n = 8$. As the offset increases, the amplitude increases to a maximum and then decreases. For $n = 8$, the maximum amplitude occurs near $\rho/H = 20$. At $\rho/H = 50$, the amplitude for $n = 8$ is larger than for any other n value. As the offset increases, the amplitude of the later arrivals increases and the number of arrivals within a fixed time interval increases. When the wavelets are partially resolved, this causes additional wiggles to appear on the tail of the first event ($m = 0$).

As the offset increases, the time delay decreases for each n value. The wavelet associated with each reflection moves forward in time with respect to the onset, and the amplitude of the early arrivals decreases. It is this behavior which is responsible for shingling.

It may seem odd that at a given offset, the amplitude actually increases as the number of reflections increases. For $m = 0$ the amplitude is determined by

$$A_{n,\rho} = T_{P_1P_2} T_{P_2P_1} R_{PP}^{n-1}.$$

At the critical angle (θ_c), $R_{PP} = 1$ and $T_{P_1P_2} = 0$. As θ decreases, R_{PP} decreases rapidly and is always less than unity. This means that the amplitude reaches a maximum value near θ_c and that the position of the maximum migrates toward θ_c as n increases.

In Figure 10, $A_{\eta,\rho}$ is plotted as a function of $V_1/V_2 - \sin\theta$ for several η values. If the angle of incidence were independent of η, the amplitude would decrease with increasing η. Actually, increasing η causes the angle of incidence to decrease. This fact and the proximity to the critical angle of the peaks for the higher η values explain the increase in amplitude with increasing η. The dashed lines are drawn for particular ρ/H values.

THE REFRACTED ARRIVAL

The reflected waves and head waves superpose to form the refracted arrival. The actual response function is obtained by (a) convolving the source function with the sequence of impulses which represent the reflected waves and (b) convolving the integral of the source function with the sequence of impulses which represent the head waves (as indicated in Equation (11)). The choice of source function is not completely arbitrary. It must be chosen so that each point in an infinite medium returns to its original state a finite time after the arrival of the disturbance at that point. This means that the D.C. component of such quantities as the stress and strain must be finite. The Laplace transform of the radial stress in a spherically symmetric compressional wave is

$$\overline{\tau}_{rr} = -P_0 a \overline{\chi} \frac{e^{-sr/V_1}}{r} \left\{ 1 + 4\frac{r^2}{V_1^2}\left(\frac{V_1}{sr}\right) + 4\frac{r^2}{V_1^2}\left(\frac{V_1}{sr}\right)^2 \right\} .$$

In order for the D.C. component to be finite,

$$\lim_{s \to 0} \overline{\chi} = A s^{\lambda} , \quad \lambda \geq 2 . \tag{14}$$

As a consequence of (14), χ must have at least two axis crossings. We also require that the particle velocity and acceleration be continuous. One function which satisfies all these conditions is

$$\chi\left(\frac{t}{t_d}\right) = \left(\sin^2 \frac{\pi t}{K t_d}\right) \cos \frac{2\pi t}{t_d} , \quad 0 \leq \frac{t}{t_d} \leq K , \quad K \geq 2 .$$

The first factor determines the envelop. The duration of the function is $T = K t_d$. The condition $K \geq 2$ forces the low-frequency behavior to satisfy (14). The source function and its integral are plotted in Figure 11 for $K = 4$. The source function is symmetric about $t/t_d = 2$. The integral of the source function is antisymmetric about $t/t_d = 2$. It follows that under certain conditions, we can distinguish between reflected and head wave contributions to the refracted arrival on the basis of symmetry.

Figures 12-14 show how the character of the refracted arrival varies with the dominant frequency at three offsets. In each figure, the dimensions are fixed. One division along the abscissa is equal to the dominant period. As we move down, the dominant period increases, the dominant wavelength increases, and E/λ_d decreases. Because the dominant period changes, the time scales cannot be compared directly.

If the refracted arrival consisted of the head wave only, all traces would have the antisymmetric form of the head wave and would terminate at the fourth division. Figure 12 shows three distinct events for $E/\lambda_d = 7$, 5 and 4. These events correspond to $m = 0$, 1 and 2. As E/λ_d decreases, the later events move toward the first event, interfere with it and become lost in it.

Changes in E/λ_d produce significant changes in character for ρ/H values of 3.5 and 10, but relatively minor changes for $\rho/H = 100$. At large offsets, the dominant frequency

is not high enough to partially resolve the individual waves which contribute to the first event. At small offsets, the individual waves are separated by larger time intervals and the change in character is a consequence of interference.

As we move down on each figure, the dominant period increases. This causes the individual waves to overlap to such an extent that only a single event is discernible and reduces the amplitude of the reflected waves relative to the head waves. This explains why the last trace on each figure approaches the antisymmetric shape associated with the head wave.

Each trace is normalized so that the maximum amplitude plots at the same value. The true maximum amplitude in the refracted wave train is plotted in Figure 15 as a function of the dominant wavelength to thickness ratio. Each curve is drawn for a particular offset. As the offset increases, a relative maximum develops which migrates toward the vertical line marked $t_d = T_\Delta$. We have shown that at large offsets the waves arrive in groups which are associated with different m values and are separated by the time interval T_Δ $t_d = T_\Delta$ is the condition for constructive interference between the groups. The weak minimum and maximum at $f/H = 100$ are also a consequence of interference between the groups.

As the dominant frequency increases, the individual waves in the group begin to separate from one another, and the amplitude varies in a complex way. Destructive interference

between individual waves is responsible for the deep minimum. At sufficiently high frequencies, the individual waves are completely resolved and each curve must approach an asymptote with slope -1/2. At very low frequencies, the head wave is dominant and each curve must approach an asymptote with slope 1/2. The increase in amplitude at low frequencies is indicative of the failure of the high-frequency theory. If this increase in amplitude were continued to very low frequency, the energy in the refracted wave would exceed the total energy radiated into the system (E_T). There is also another indicator of the failure of the asymptotic theory. We are dealing with a layer which is embedded between two half-spaces which have identical properties. In the limit as the layer thickness goes to zero, the amplitude of the refracted arrival must go to zero. The multiply reflected waves exhibit the correct behavior (Equation 13), but the head wave amplitudes do not go to zero (8). We do not attach significance to dominant wavelength to thickness ratios greater than unity; consequently, this analysis is restricted to thick high velocity zones.

Figures 16-18 illustrate the effect of offset. On each figure, the E/λ_d ratio is constant and the dominant period does not change from trace to trace. Each trace is normalized so that the maximum amplitude plots at the same value. The normalized offset (ρ/H) changes in increments of 0.5. The group of lines which start in the upper left corner of Figure 16 show how the

individual peaks and troughs move forward with respect to the onset and decrease in amplitude as the offset increases. This behavior is known as shingling. The decrease in amplitude would be considerably more pronounced if true amplitudes had been plotted.

In their model experiments, Levin and Ingram (1962) observed that the phase velocity measured as a function of layer thickness takes on values which exceed the compressional velocity in the layer. The explanation for this effect lies in the fact that the phase velocity of the reflected waves exceeds the compressional velocity in the layer. The effect is not observed when the layer is very thick because the initial peaks and troughs are associated with the true head wave which is observed uncontaminated by reflections off the bottom of the layer. For thin layers the effect is not observed because the phase velocity of the reflected waves approaches the compressional velocity in the layer.

The second group of lines in Figure 18 show how additional peaks and troughs appear on the tail of the first event as the offset increases. These phases are associated with the later arriving, higher η values which increase in amplitude with offset. The third group of lines shows that shingling also occurs in the second event ($m = 1$).

The shingling effect may be particularly pronounced when the difference between the phase velocity of the reflected waves

(C) and V_2 is large. The phase velocity is defined by

$$\frac{C_{nm}}{V_1} = \frac{d\frac{\rho}{H}}{d\frac{t_{nm}}{H/V_1}} = \frac{1}{\sin\theta_{nm}} .$$

The difference in phase velocity is

$$\frac{C_{nm}-V_2}{V_1} = \frac{\frac{V_1}{V_2} - \sin\theta_{nm}}{-\frac{V_1}{V_2}\sin\theta_{nm}} \qquad (15)$$

Changes in the physical dimensions which reduce θ_{nm} increase the phase velocity difference. Therefore, increasing the layer thickness or reducing the offset increases the phase velocity difference. Figures 16-18 were computed for a relatively thin layer (E/H = .1). For thicker layers, individual extrema move toward the onset more rapidly with increasing offset.

In Figure 17, the phase velocity is slightly greater for the third peak than it is for the earlier extrema. Shingling is exhibited only over a limited range of offsets. The second trough and third peak on the first trace can be correlated across the entire record, but the phase velocity difference disappears for $\rho/H > 7$. In Figure 18, $E/\lambda_d = 4$ and there is no shingling. These observations indicate that for a fixed dominant period, shingling is not observed beyond a certain maximum offset. The maximum offset decreases as the dominant period increases and for sufficiently long dominant periods, shingling does not occur. When shingling is observed, it indicates that the high velocity zone is thick. The lower bound on E/λ_d depends on the depth to the layer. For E/H = .1, the existence of shingling indicates that $E/\lambda_d > 4$.

Normal mode propagation in which the phase velocity exceeds the group velocity can produce shingling but not distance-limited shingling. This is because the group velocity - phase velocity relationship for a single mode is independent of distance.

The maximum amplitude and the amplitudes of individual peaks (P_i) and troughs (T_j) are plotted against offset in Figure 19. Notice how the maximum amplitude shifts to later extrema as the offset increases. The first extremum may not be observed because of noise or insufficient dynamic range. Nevertheless, in certain cases it may still be possible to determine the onset of the event. Figures 12-14 show that the position of the deepest trough is relatively insensitive to offset and to E/λ_d when E/λ_d is near unity. In each case, the deepest trough occurs at a time near $2t_d$ after the onset. Recall that $2t_d$ is the time at which the source function takes on its maximum value. This suggests that the time of the source function maximum might determine the delay factor to be used in determining the true onset of the refracted arrival. When used in this way, the source function should include the effect of reverberation in the near surface in the vicinity of the source and receiver.

In Figure 20, the maximum amplitude is plotted against offset for different values of E/λ_d. Changes in the way in which the individual wavelets interfere accounts for the complicated variation of the higher frequency curves. For E/λ_d values of

4 and 7, the amplitude actually increases with offset over limited ranges of ρ/H. For $\rho/H > 8.5$, the maximum amplitude occurs for $E/\lambda_d = 1$. At large offsets ($\rho/H > 20$), each of the curves approaches the $(\rho/H)^{-3/2}$ decay required by (13).

CONCLUSIONS

At large offsets the refracted arrival from a layer results from a superposition of all waves which travel with phase velocities equal to or near the compressional velocity in the layer. This requirement is satisfied by the head waves generated by reflected waves which do not cross the layer in the compressional mode and by multiply reflected waves which cross the layer at least once in the compressional mode. Specifying n (the number of crossings in the compressional mode) and m (the number of crossings in the shear mode) does not define a particular ray but rather a family of degenerate rays which arrive at exactly the same time. The number of rays in the family is

$$D_{nm} = (n+m)!/n!m! .$$

The individual rays differ from one another in the sequence in which the P and S legs of the path are traversed. Because all the rays arrive at exactly the same time, only the total amplitude is physically significant. A formula is derived which gives the total amplitude in terms of a series which contains either m or $n + 1$ terms (whichever is smaller). This formula makes possible the rapid computation of highly degenerate events.

The travel-time curves for all rays with the same m value approach the same asymptote regardless of the n values. The travel-time curves for waves with different m values approach

asymptotes which differ by a multiple of T_Δ . At large offsets and for thin layers, the total amplitude obtained by summing all rays with the same m value satisfies

$$A_m = \gamma_m (\rho/H)^{-3/2} (E/H)^{1/2} .$$

The head waves decay with distance like $(\rho/H)^{-2}$. Therefore, tne reflected waves predominate at large offsets. The reflected waves also predominate when the dominant frequency is high. If the duration of the source function is less than T_Δ , the refracted arrival consists of a series of events. Each event is associated with waves which cross the layer the same number of times in the shear mode. At large offsets the onsets of the events are separated by T_Δ , the phase velocities approach the compressional velocity in the layer, the amplitudes decay like $(\rho/H)^{-3/2}$ an. the relative amplitudes are determined by the γ_m . The γ_m depend only on the density and velocity ratios. The higher orders $(m>0)$ are shown to be significant when the compressional velocity contrast is large, the Poisson's ratio in the layer is near .25 or the Poisson's ratio in the infinite medium approaches .5.

The multiply reflected waves propagate with phase velocities which exceed the compressional velocity in the layer. Consequently, as the offset increases, each wavelet moves toward the beginning of the refracted arrival. In this process the early arrivals (corresponding to the smaller n values) decrease in amplitude. The slightly higher phase velocity and the decrease

in amplitude produce the shingling effect. The later arrivals (corresponding to higher n values) first increase and then decrease in amplitude. This causes additional wiggles to appear on the tail of each event as the offset increases. The shingling is distance-limited. The maximum offset at which it is observed decreases with increasing period, and for sufficiently long period it is not observed. Shingling occurs when the high velocity zone is thick compared with the dominant wavelength. We know that the smallest value of (E/λ_d) for which it occurs depends on E/H and that as E/H increases, the shingling effect becomes more pronounced.

For E/λ_d near unity, the time of the deepest trough is not very sensitive to changes either in offset or in E/λ_d. In our case the time between the onset of the refracted wave and the deepest trough is determined by the time at which the source function attains its maximum value. If this were true generally, it would provide a means for making a good estimate of the onset time. When used in this way, the source function must include the effect of reverberation in the near surface in the vicinity of the source and receiver.

Beyond a certain offset, the maximum amplitude of the refracted arrival occurs for $\tau_d = T_\Delta$. This is the condition for constructive interference between the groups of waves corresponding to different n values.

Our results have been obtained by using high-frequency geometric ray theory and approximate the exact theory for $E/\lambda_q \geqq 1$.

Reflections off interfaces both above and below the high-velocity zone can introduce energy into the layer at and near the critical angle to produce secondary refractions. A reflection off a deeper interface can generate a secondary refraction when the interface dips in such a way as to reduce the phase velocity in the reflected wave. It follows that more than one refracted arrival may be associated with one high-velocity layer. When this happens, the difference in travel times between the primary and secondary determines the travel time along the critical angle to an underlying or overlying reflector.

ACKNOWLEDGMENTS

I wish to thank Mr. Raymond Ellis for writing the computer program, for determining the source of some extremely subtle errors, and for suggesting various ways for improving the operating efficiency of the program.

This work was supported by the Air Force Cambridge Research Laboratories Contract AF 19(604)-8344 as part of the Advanced Research Project Agency's Project VELA-UNIFORM.

REFERENCES

Arons, A. B., and D. R. Yennie, Phase distortion of acoustic pulses obliquely reflected from a medium of higher sound velocity, J. Acoust. Soc. Am., 22, 231-237, 1950.

Berckhemer, H., and J. Oliver, Zur deutung seismischer einsätze mit parallelen laufzeitkurven, Zeitschrift für Geophysik, 21, 152-164, 1955.

Cagniard, L., Reflection and refraction of progressive seismic waves, translated by E. A. Flinn and C. H. Dix, McGraw-Hill Book Co., New York, 1961.

Dix, C. H., The seismic head pulse, reflection and pseudo-reflection pulses, J. Geophys. Res., 66, 2945-2951, 1961.

Donato, R. J., Amplitude of P-head waves, J. Acoust. Soc. Am., 36, 19-25, 1964a.

Donato, R. J., Head waves from liquid layers, J. Acoust. Soc, Am., 36, 26-31, 1964b.

Dunkin, J. W., A study of two-dimensional head waves in fluid and solid systems, Geophysics, 28, 563-581, 1963.

Erdelyi, A., Asymptotic expansions, Dover Publications, New York, 1956.

Garvin, W. W., Exact transient solution of the buried line source problem, Proc. Roy. Soc. London, A, 203, 528-541, 1956.

REFERENCES (Continued)

Gilbert, F., and S. J. Laster, Excitation and propagation of pulses on an interface, Bull. Seismological Soc. Am., 52, 299-319, 1962.

Heelan, P. A., On the theory of head waves, Geophysics, 18, 871-893, 1953.

Lavergne, M., Etude sur modele ultrasonique du probleme des couchès minces en sismique refraction, Geophys. Prospecting, 9, 60-73, 1961.

Levin, F. K., and J. D. Ingram, Head waves from a bed of finite thickness, Geophysics, 27, 753-765, 1962.

McDonal, F. J., F. A. Angona, R. L. Mills, R. L. Sengbush, R. G. Van Nostrand and J. E. White, Attenuation of shear and compressional waves in Pierre shale, Geophysics, 23, 421-439, 1958.

Spencer, T. W., The method of generalized reflection and transmission coefficients, Geophysics, 25, 625-641, 1960.

Strick, E., Propagation of elastic wave motion from an impulsive source along a fluid/solid interface, Phil. Trans. Roy. Soc. London, A, 251, 465-523, 1959.

BLANK PAGE

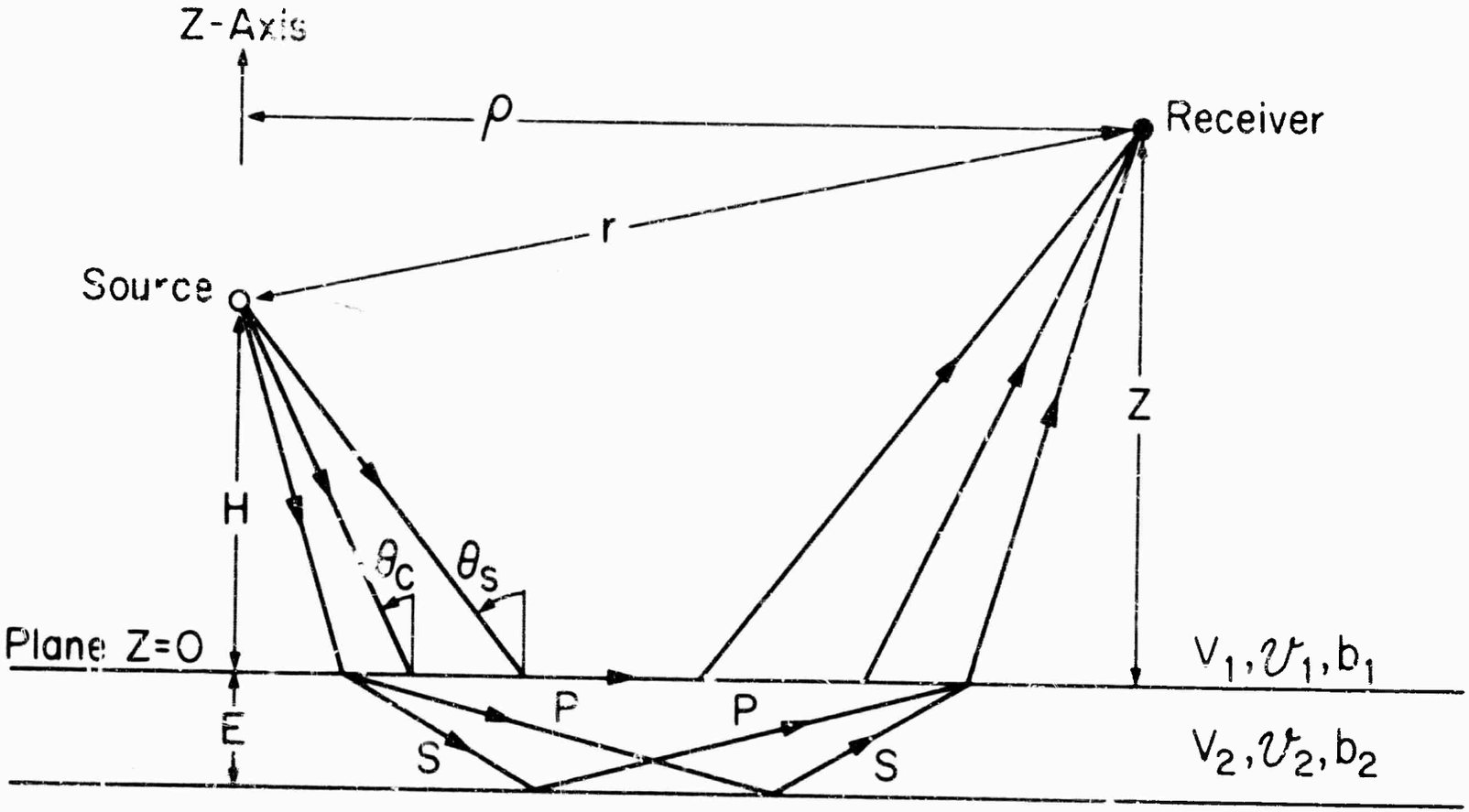

$$\theta_c = \sin^{-1} V_1/V_2,\ V_1 < V_2$$

$$\theta_s = \sin^{-1} V_1/\upsilon_2,\ V_1 < \upsilon_2$$

FIGURE 1

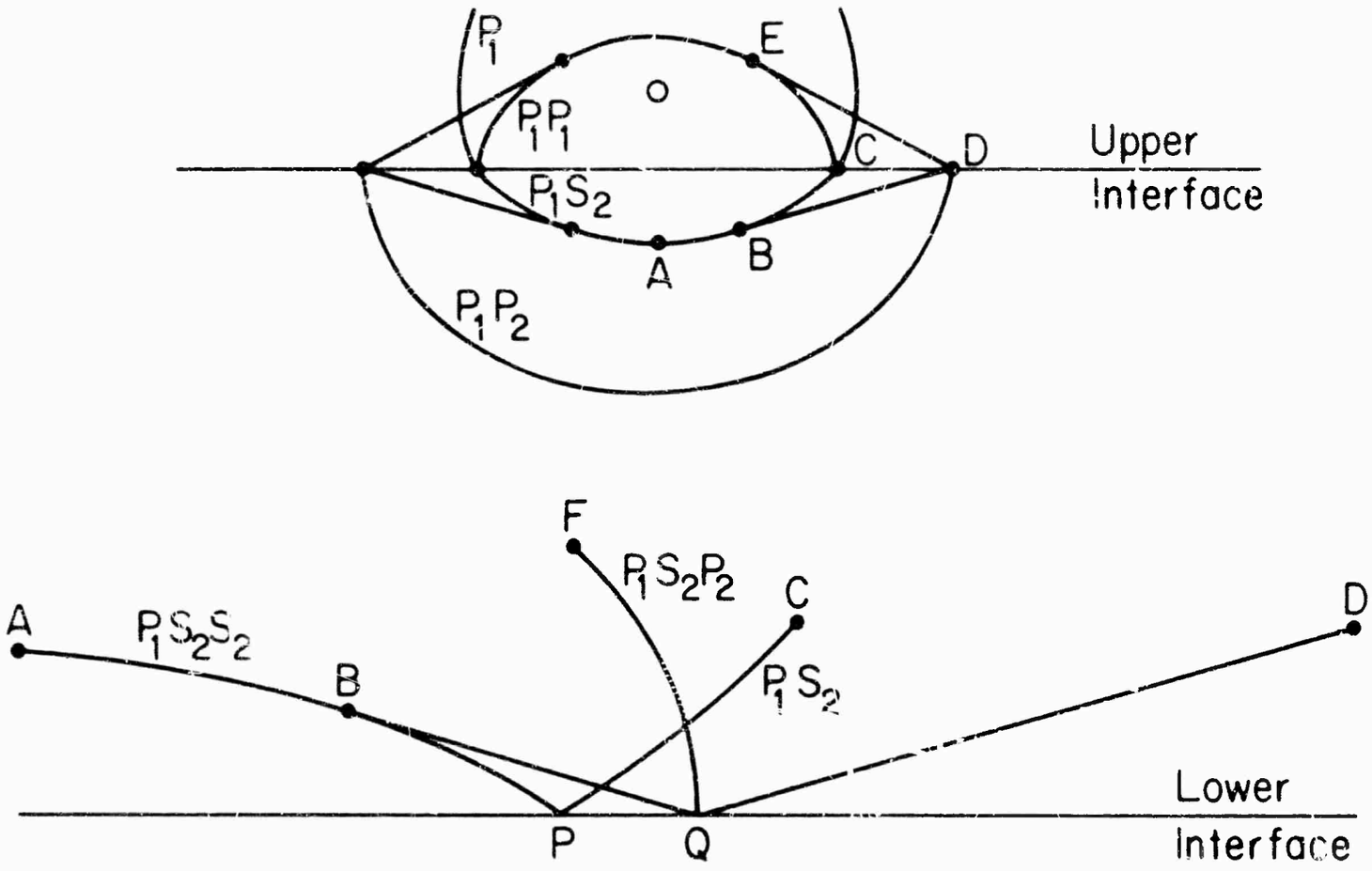
P1
E
O
P1P1
C
D
Upper
Interface
P1S2
A
B
P1P2
F
P1S2P2
C
D
A
P1S2S2
B
P1S2
Lower
Interface
P
Q

FIGURE 2

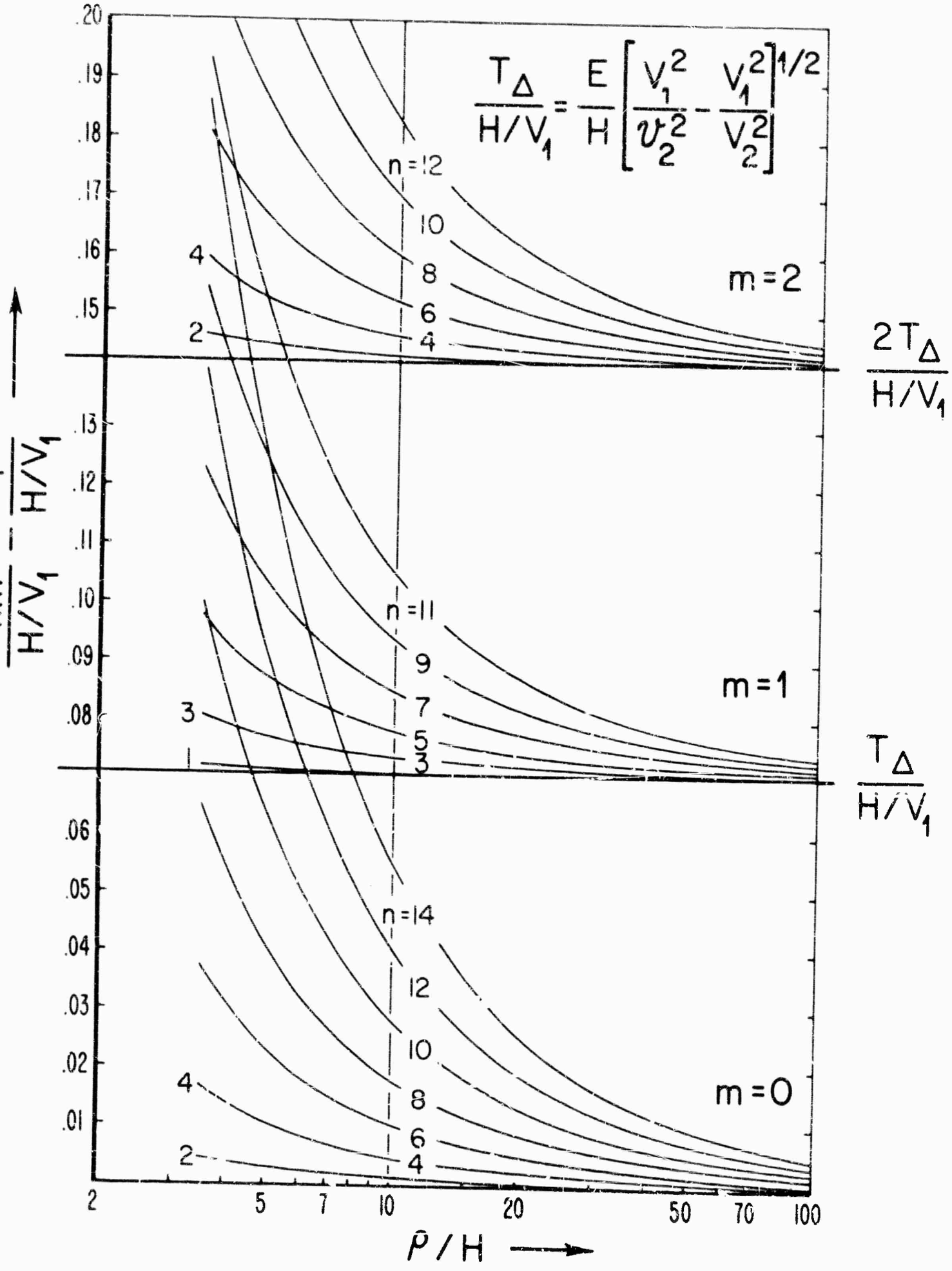

FIGURE 3

LD 44-437

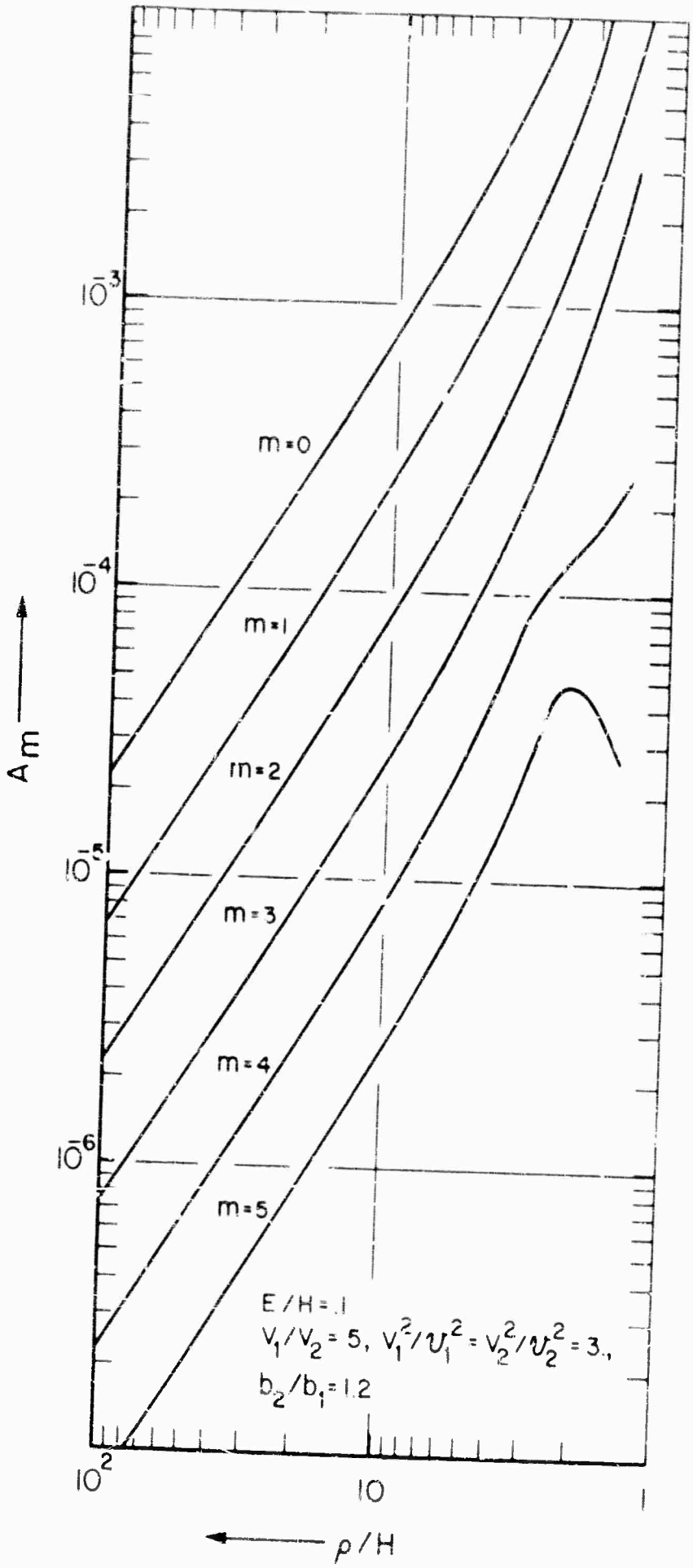
10^{-3}
10^{-4}
10^{-5}
10^{-6}
A_m
m=0
m=1
m=2
m=3
m=4
m=5
E/H=.1
$V_1/V_2 = 5,\ V_1^2/v_1^2 = V_2^2/v_2^2 = 3.,$
$b_2/b_1 = 1.2$
10^2
10
1
ρ/H

FIGURE 4

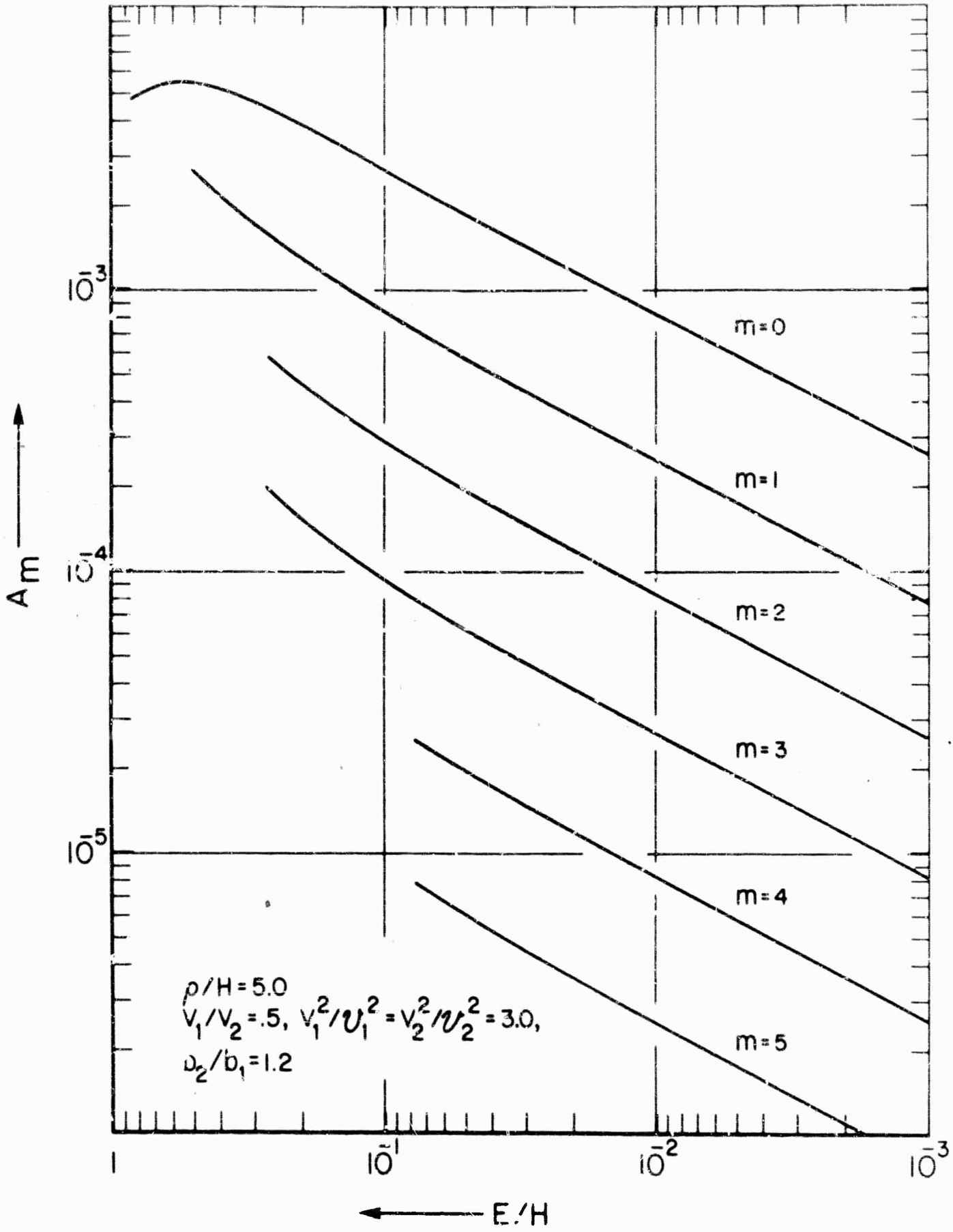
10^{-3}
10^{-4}
10^{-5}
Am
m=0
m=1
m=2
m=3
m=4
m=5
ρ/H=5.0
$V_1/V_2=.5$, $V_1^2/U_1^2=V_2^2/U_2^2=3.0$,
$a_2/b_1=1.2$
1
10^{-1}
10^{-2}
10^{-3}
E/H

FIGURE 5

BLANK PAGE

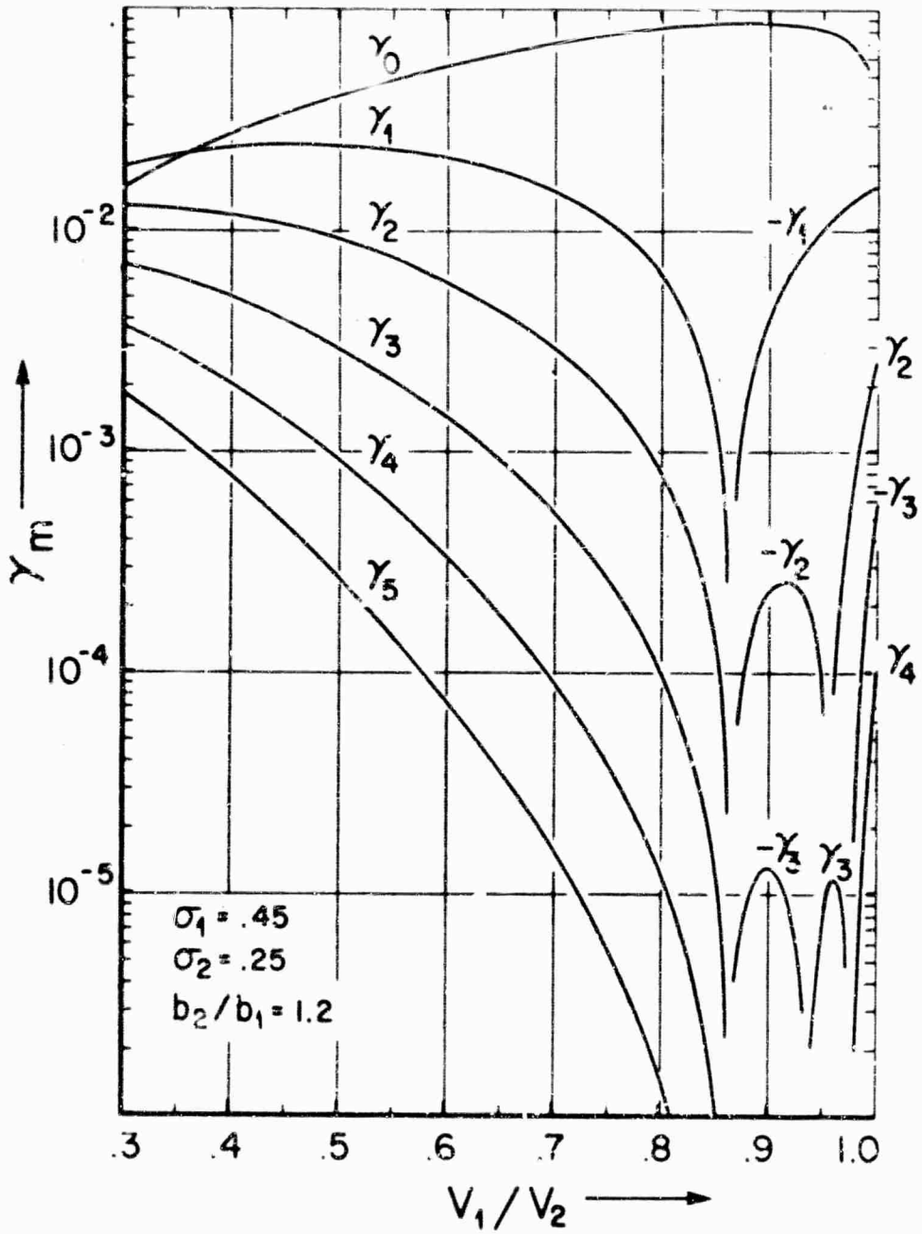

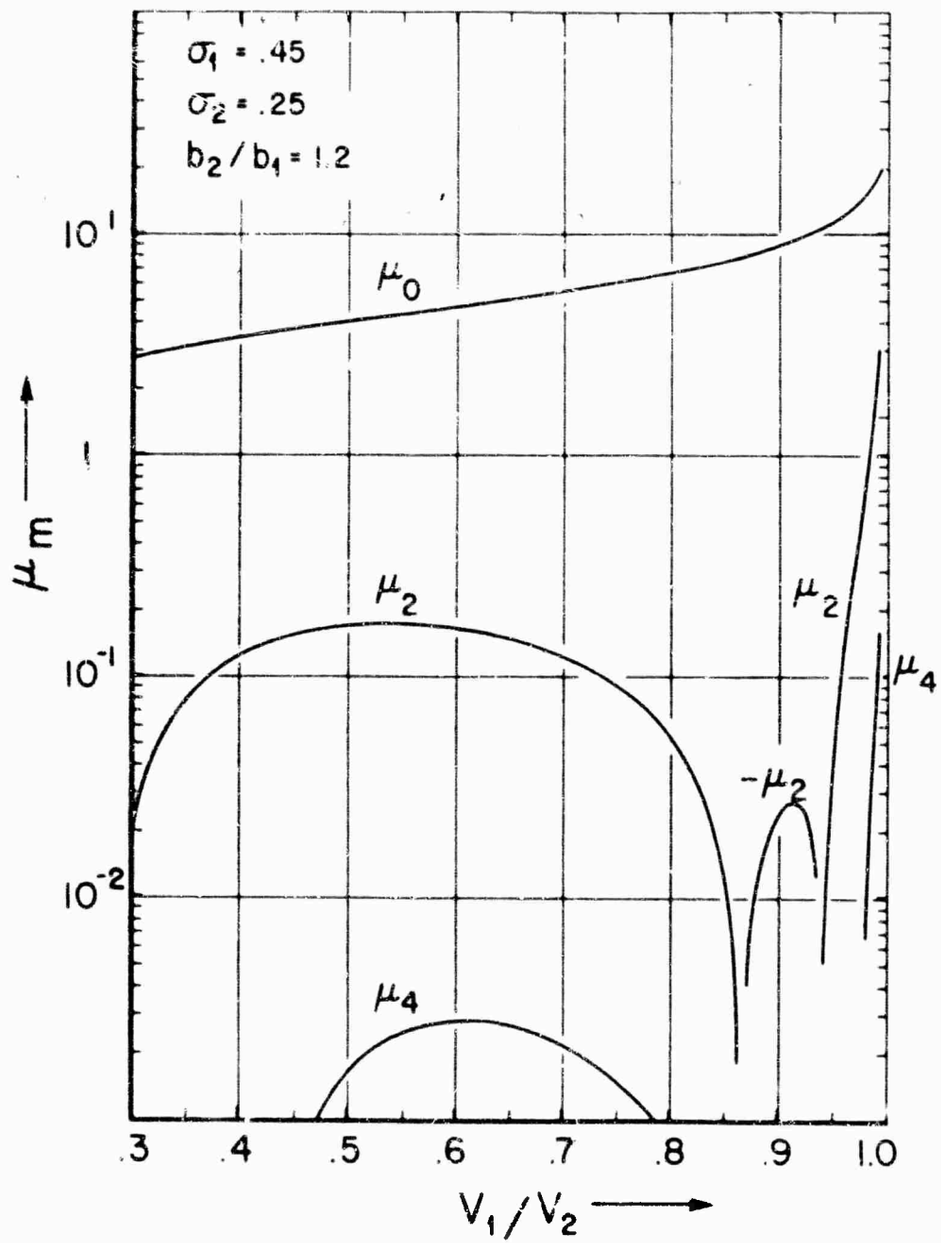

FIGURE 6

LC 44-370

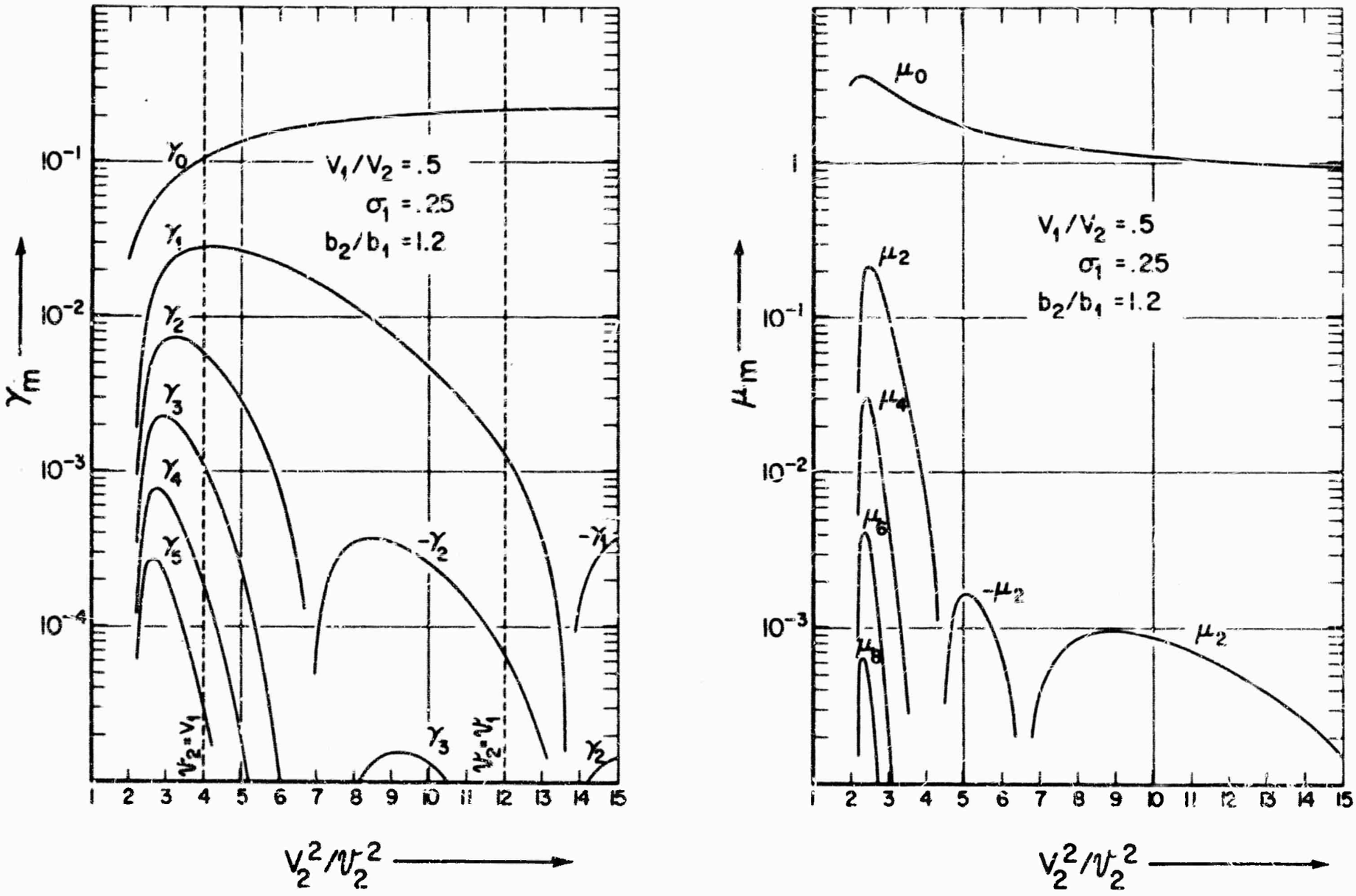

FIGURE 7

LC44-433

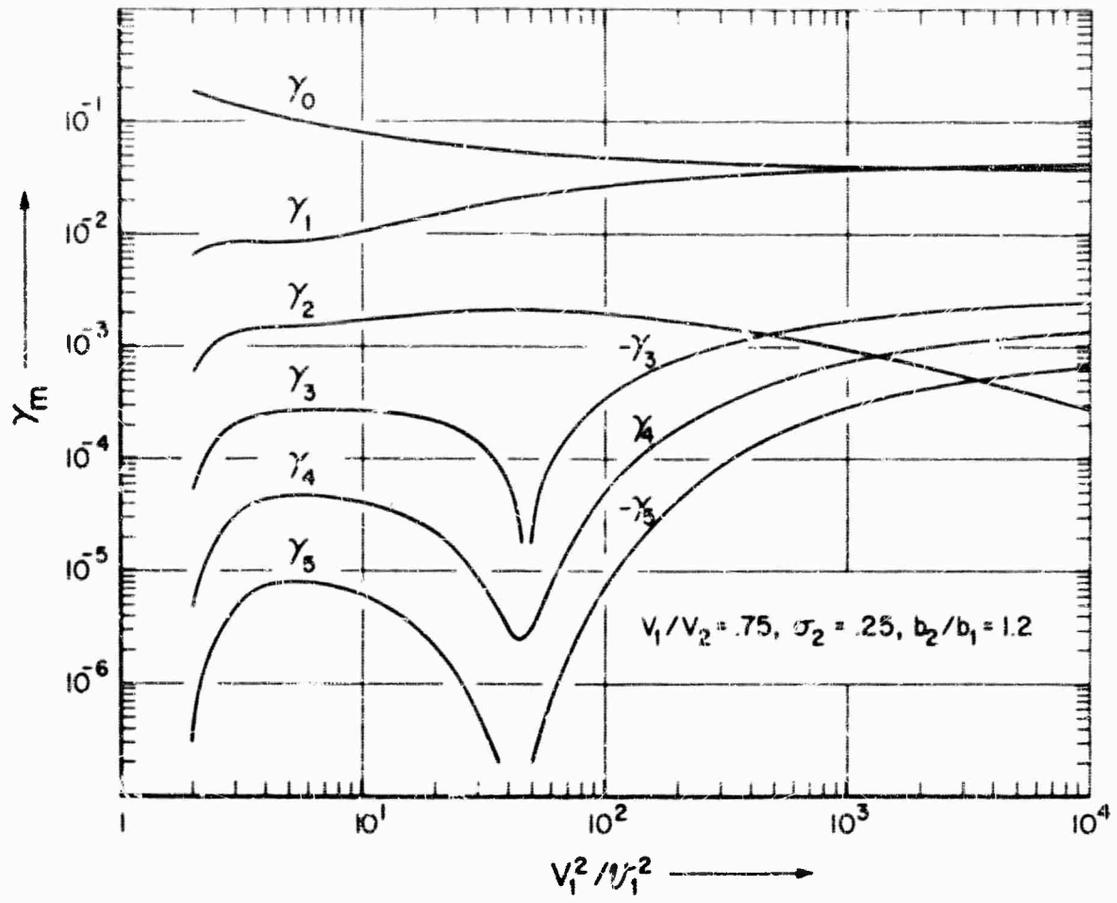
γ_0
γ_1
γ_2
$-\gamma_3$
γ_3
γ_4
$-\gamma_5$
γ_4
γ_5
γ_m
10^{-1}
10^{-2}
10^{-3}
10^{-4}
10^{-5}
10^{-6}
$V_1/V_2 = .75,\ \sigma_2 = .25,\ b_2/b_1 = 1.2$
1
10^1
10^2
10^3
10^4
V_1^2/V_1^2

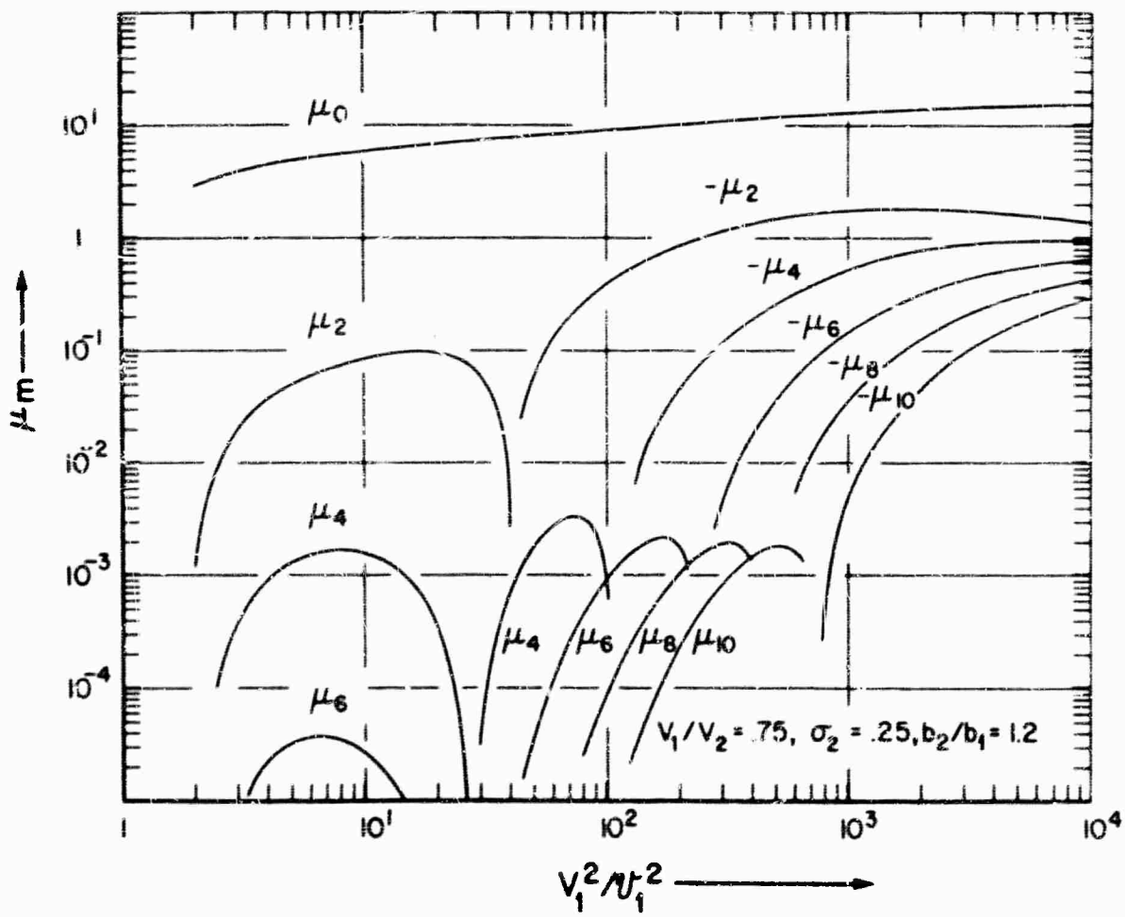
μ_0
$-\mu_2$
$-\mu_4$
$-\mu_6$
$-\mu_8$
$-\mu_{10}$
μ_2
μ_4
μ_6
μ_4 μ_6 μ_8 μ_{10}
μ_m
10^1
1
10^{-1}
10^{-2}
10^{-3}
10^{-4}
$V_1/V_2 = .75,\ \sigma_2 = .25, b_2/b_1 = 1.2$
1
10^1
10^2
10^3
10^4
V_1^2/V_1^2

FIGURE 8

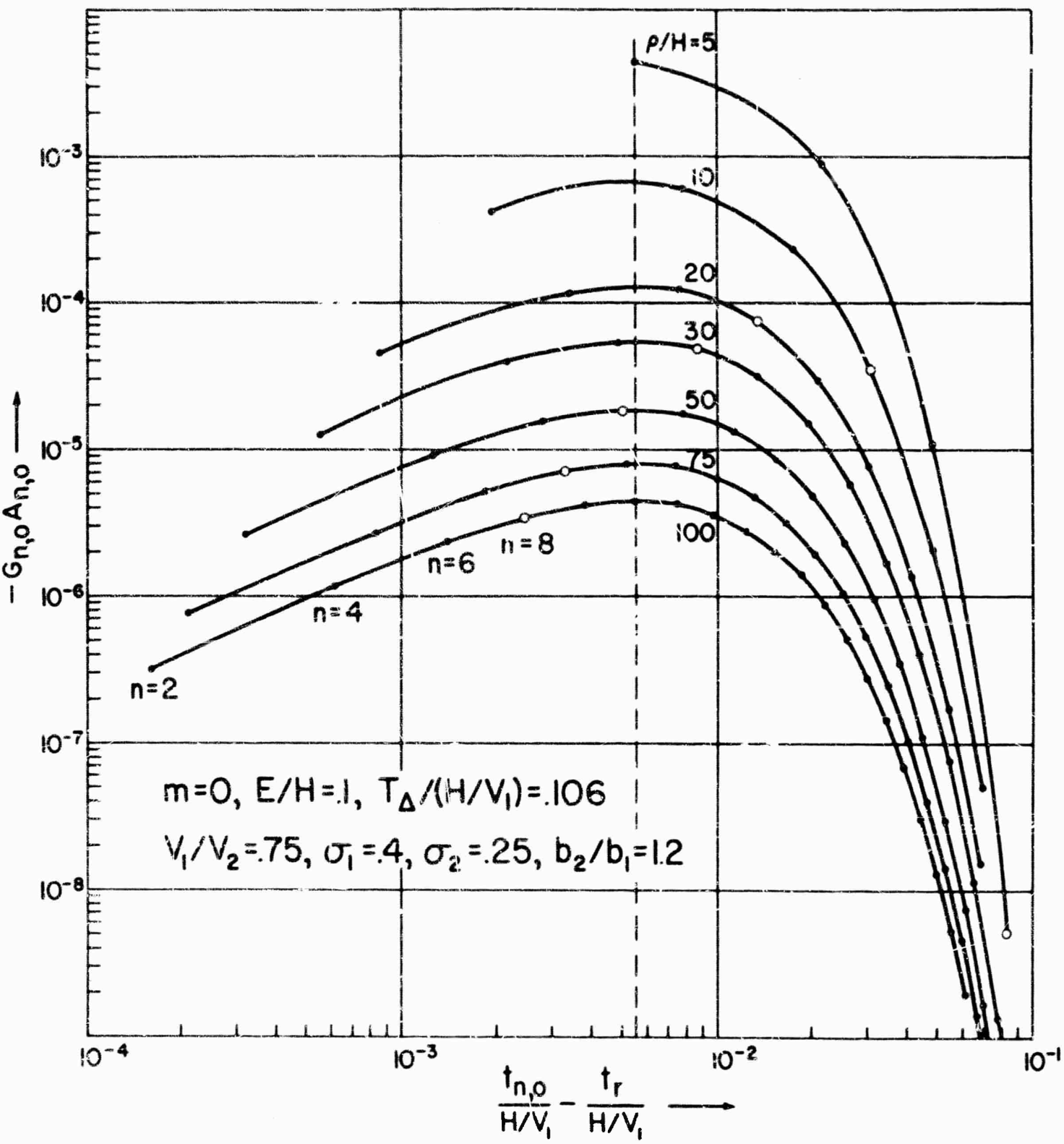

FIGURE 9

LC 44-373

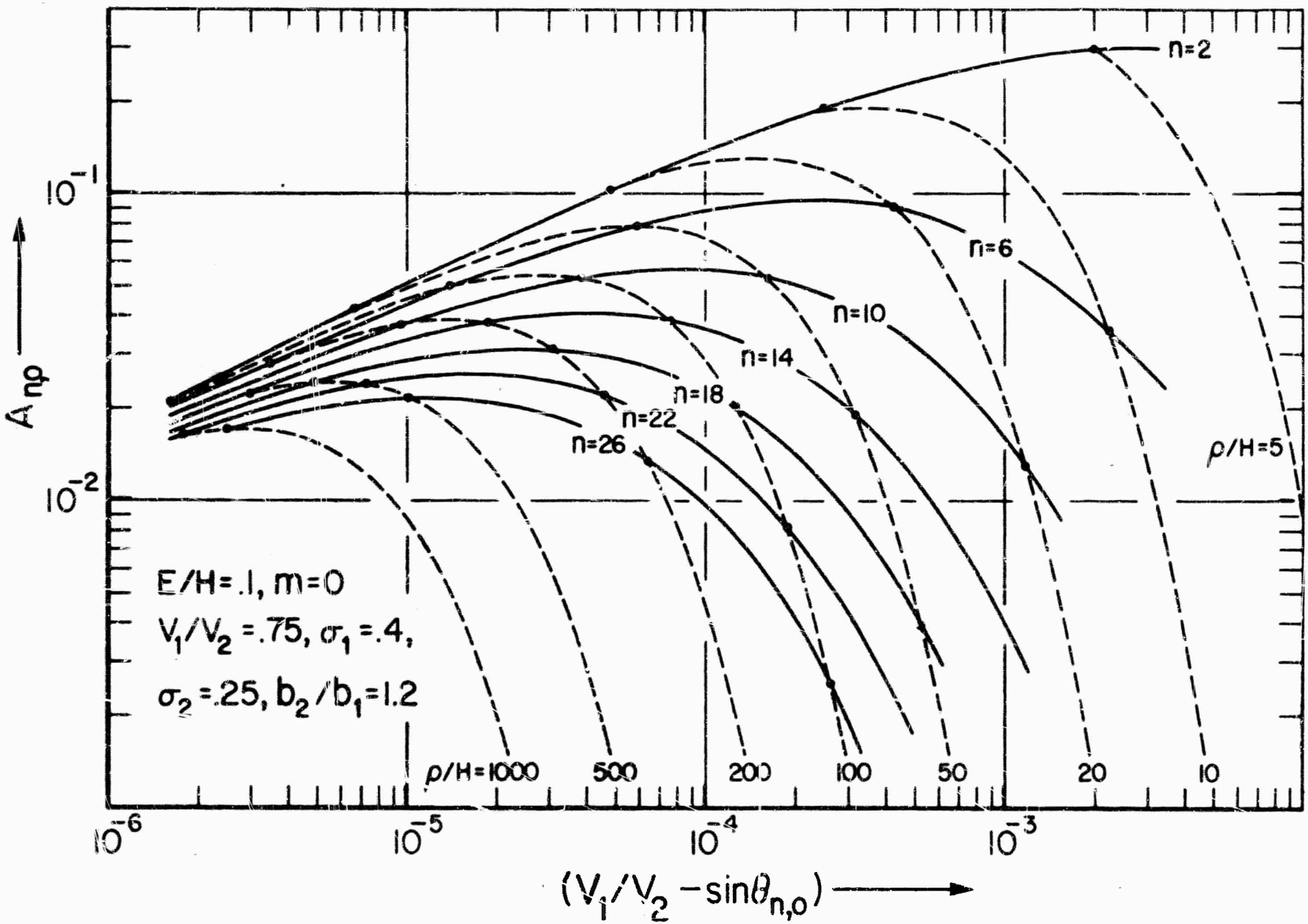

FIGURE 10

LD 44-440

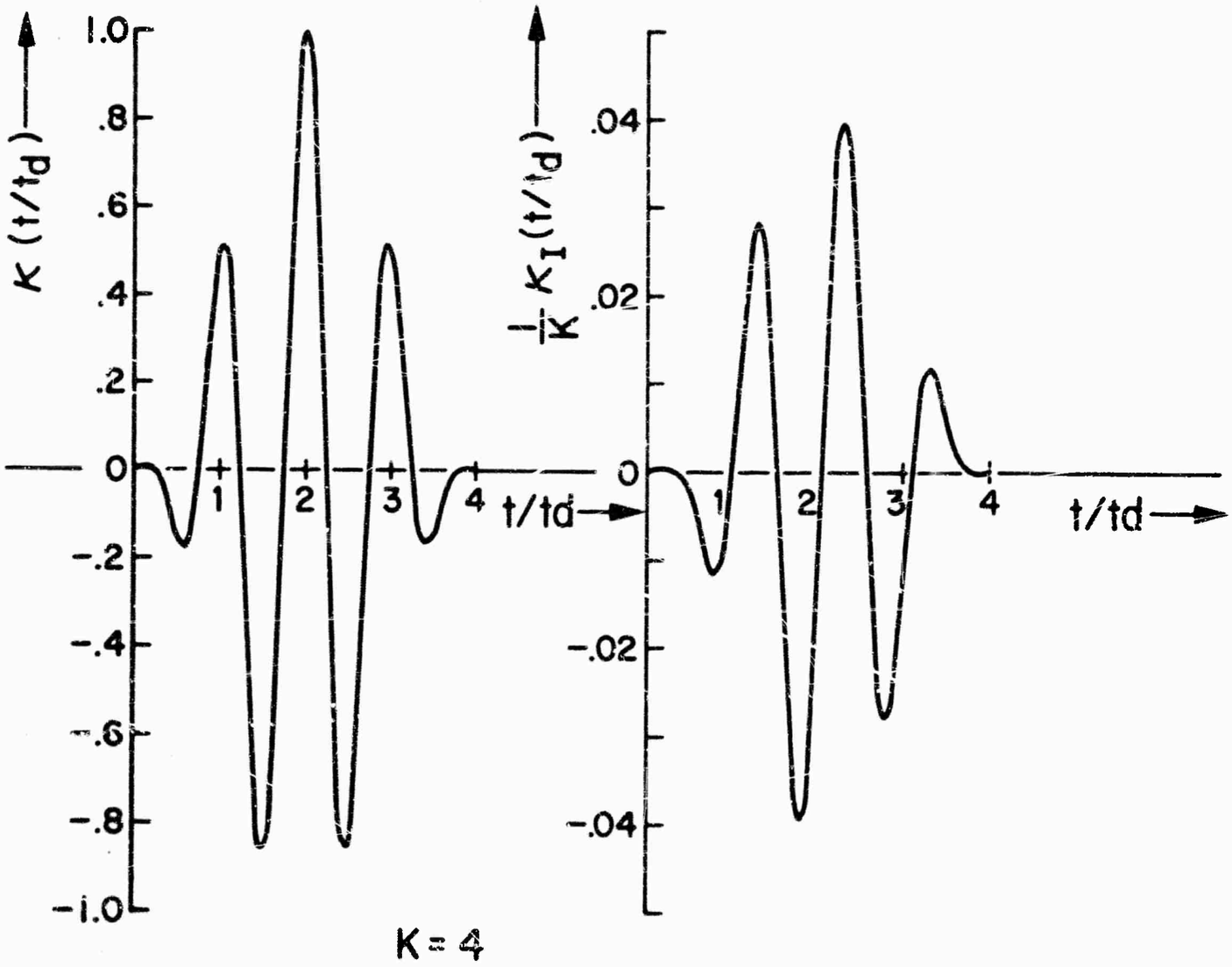

FIGURE 11

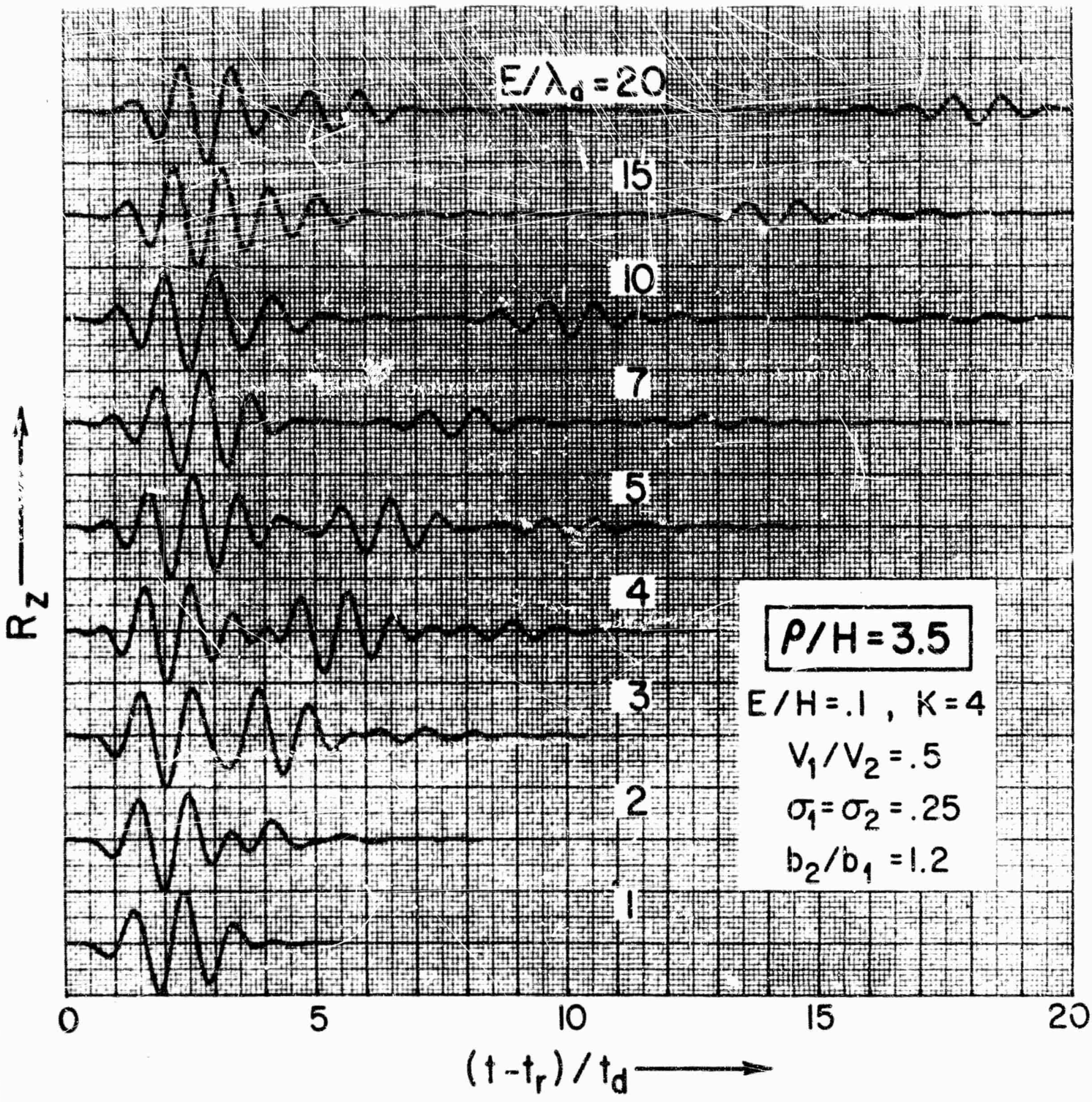

FIGURE 12

LD44-444

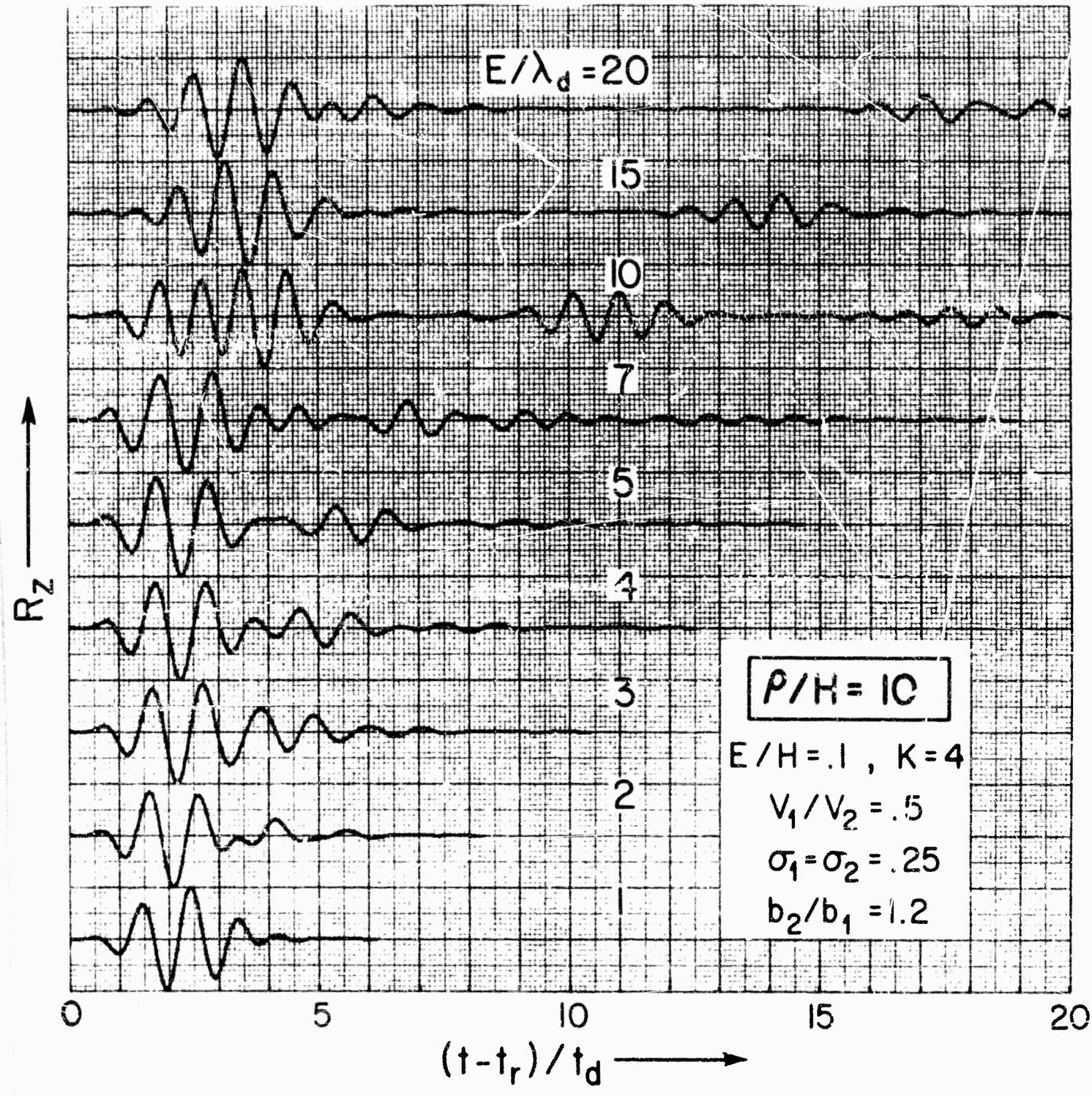

FIGURE 13

LD44-445

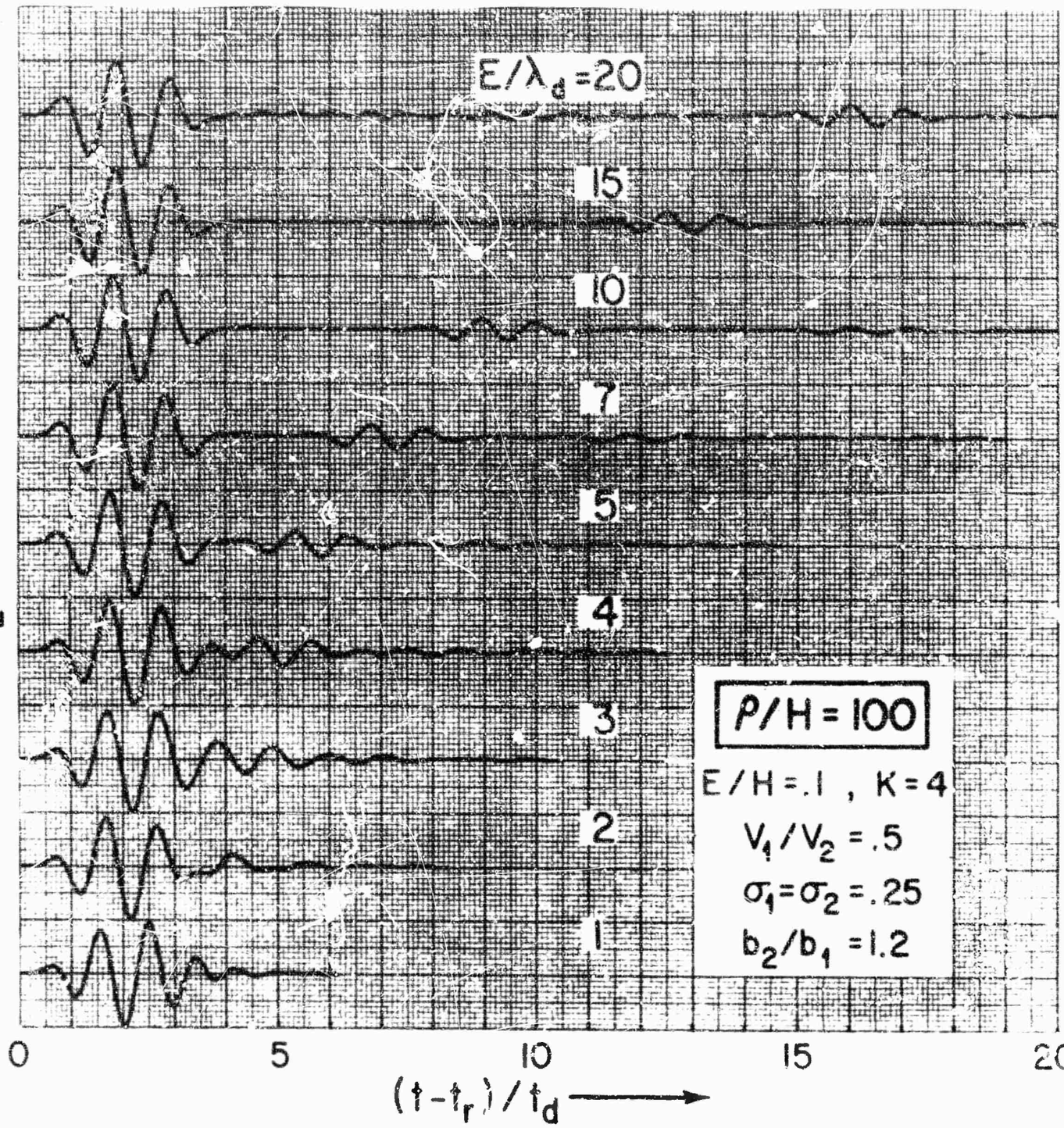

FIGURE 14

LD 44-446

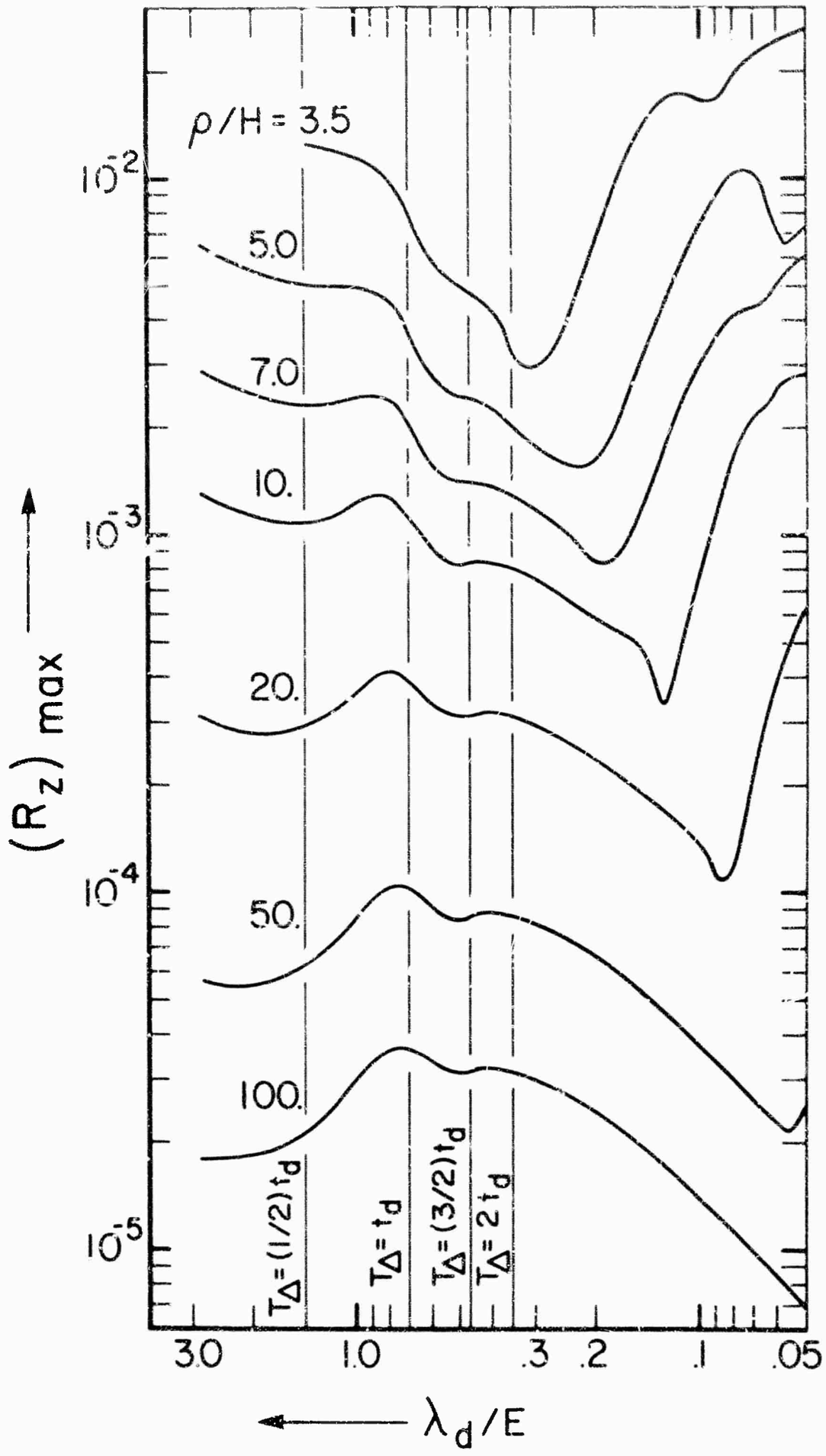

E/H = .1, K = 4

$V_1/V_2 = .5$, $\sigma_1 = \sigma_2 = .25$, $b_2/b_1 = 1.2$

FIGURE 15

LC44-372

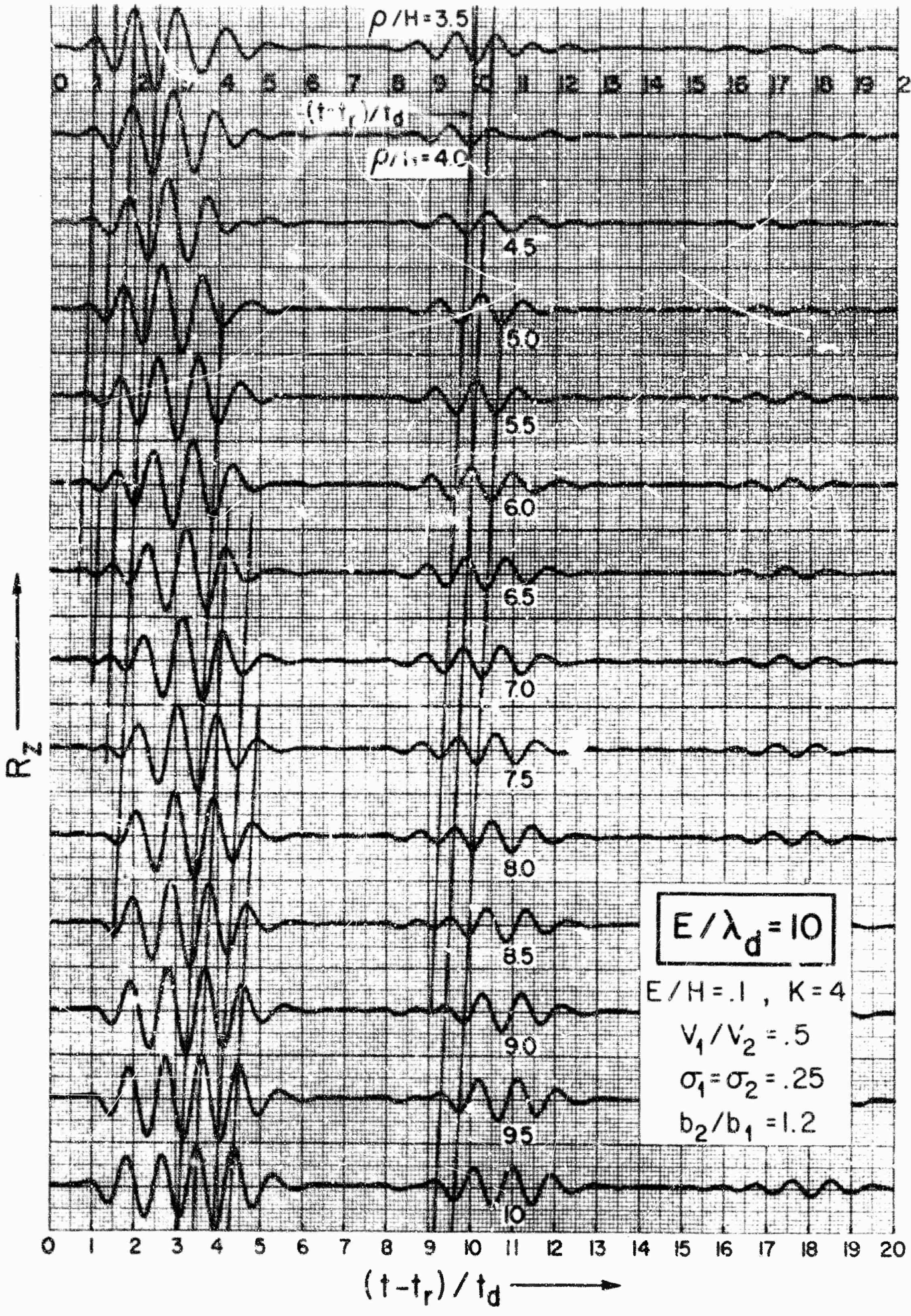

FIGURE 16

LC 44-447

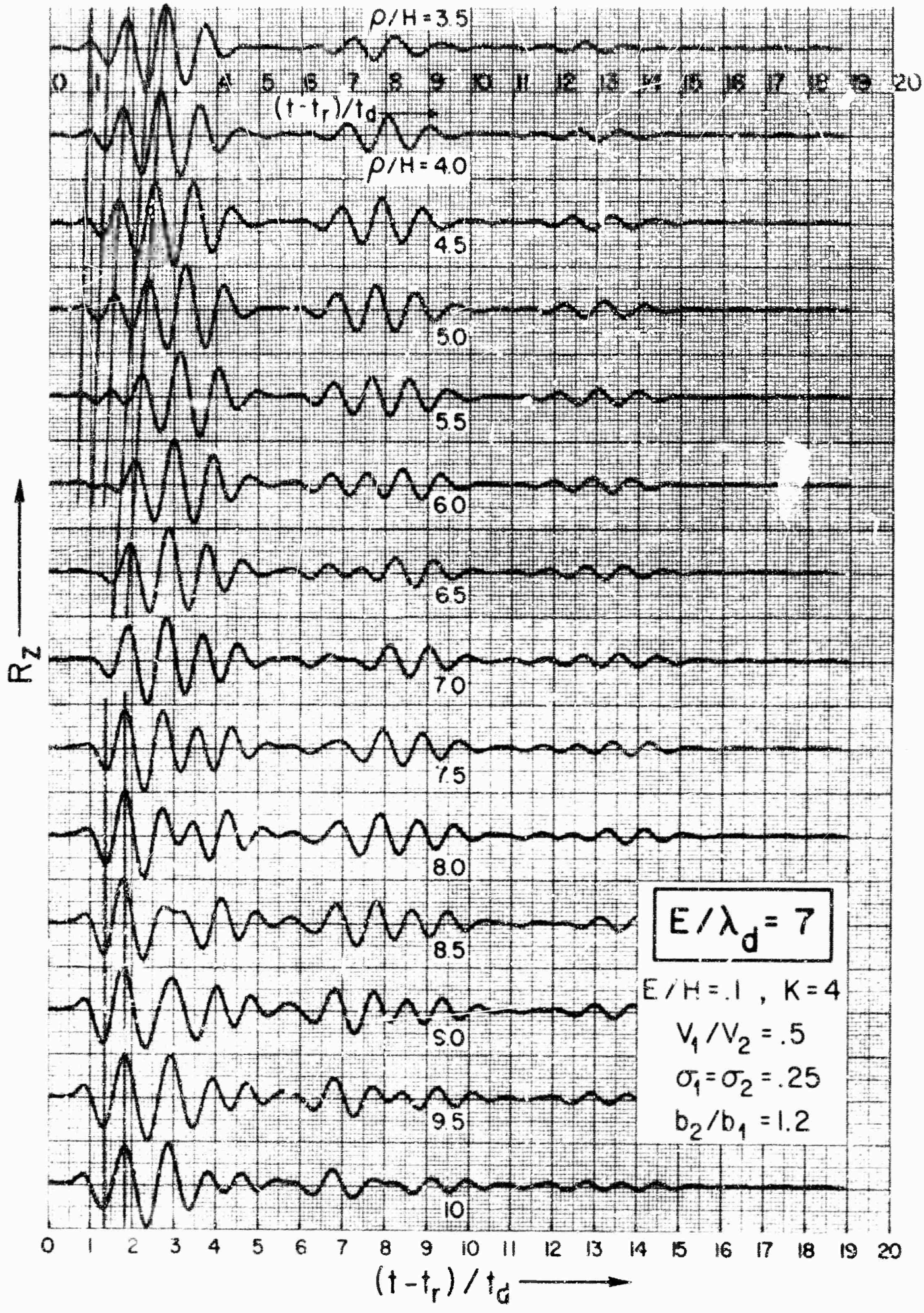

FIGURE 17

LD44-446

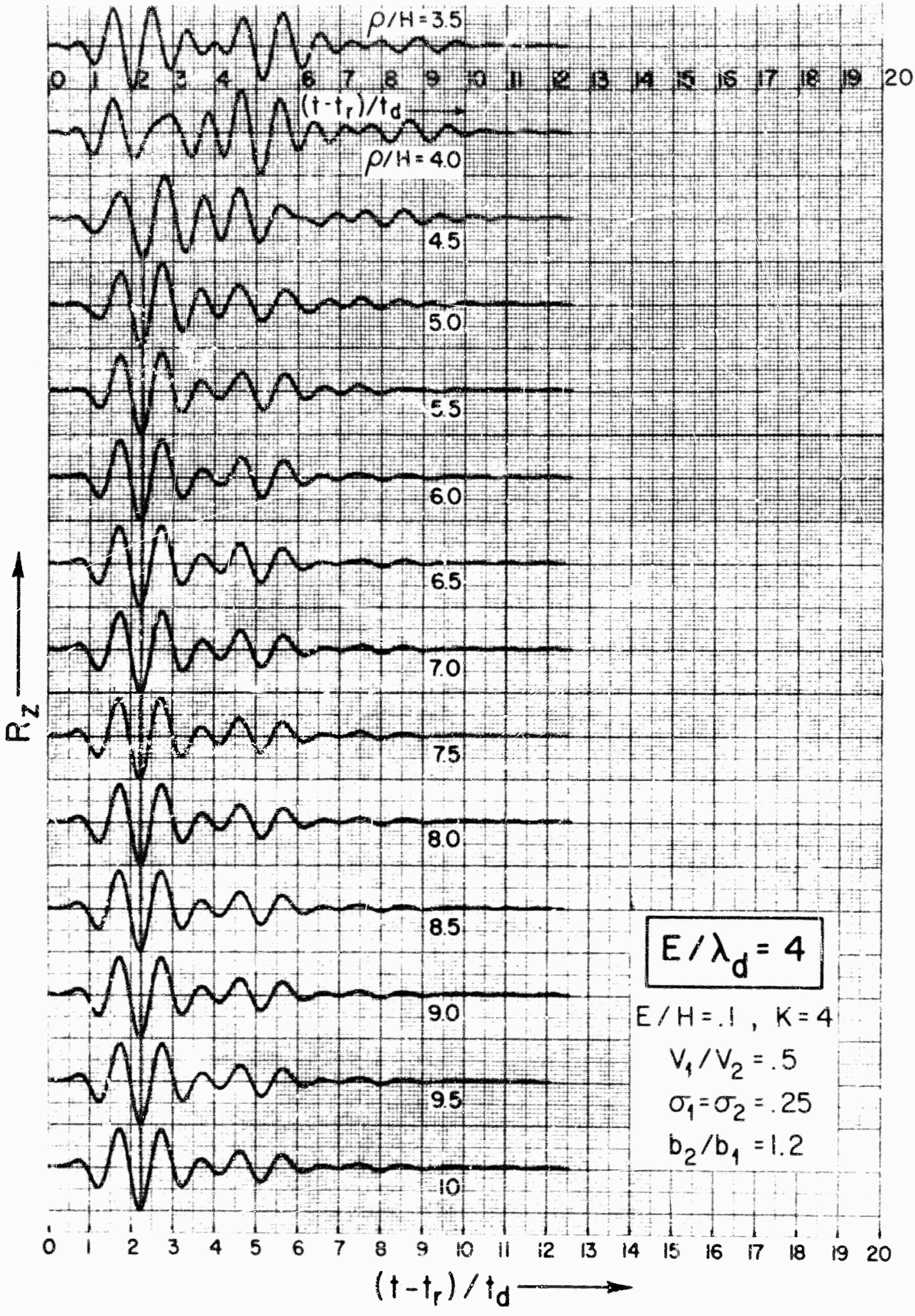

FIGURE 18

LD44-449

BLANK PAGE

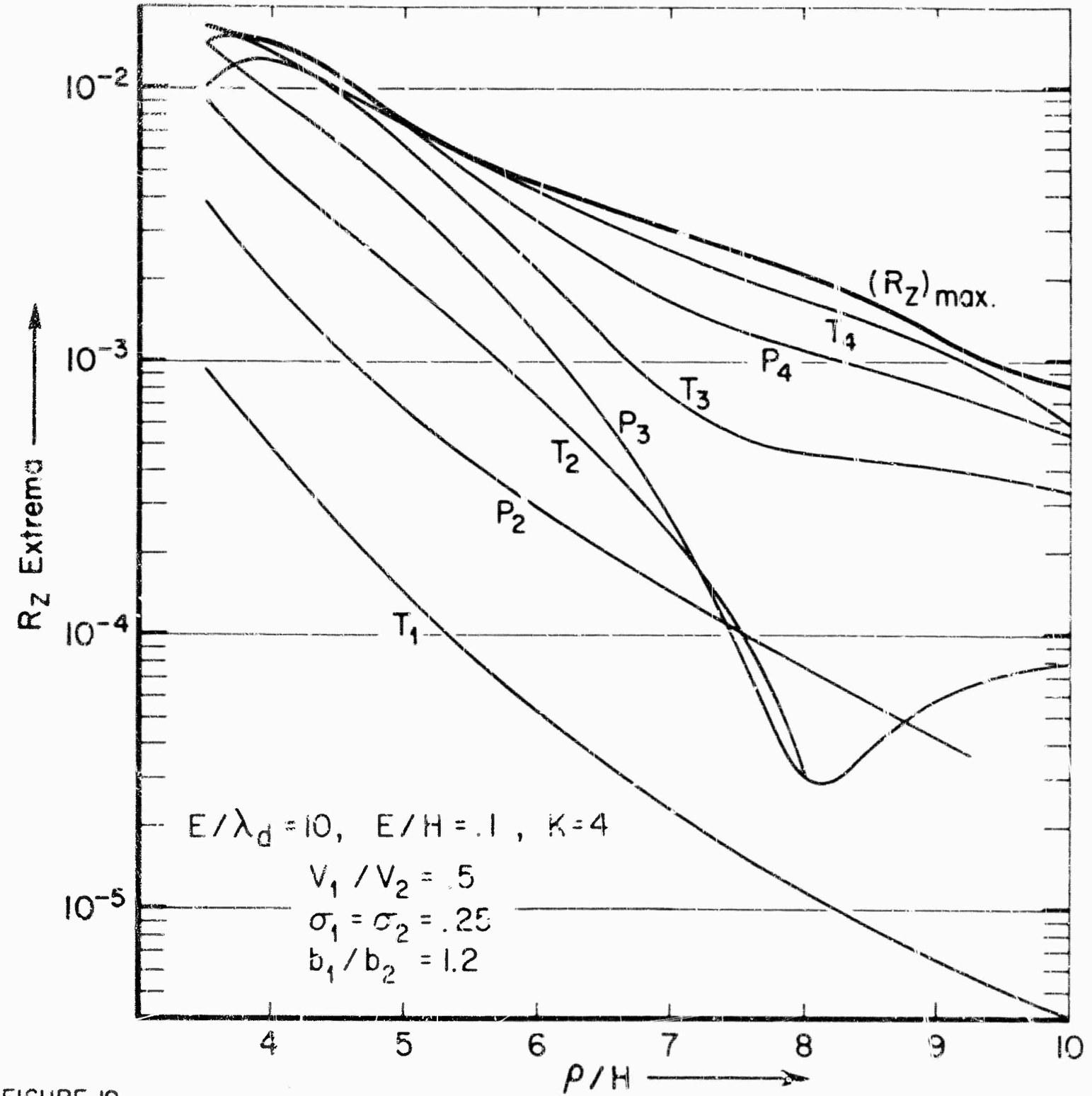

FIGURE 19

LE 44-442

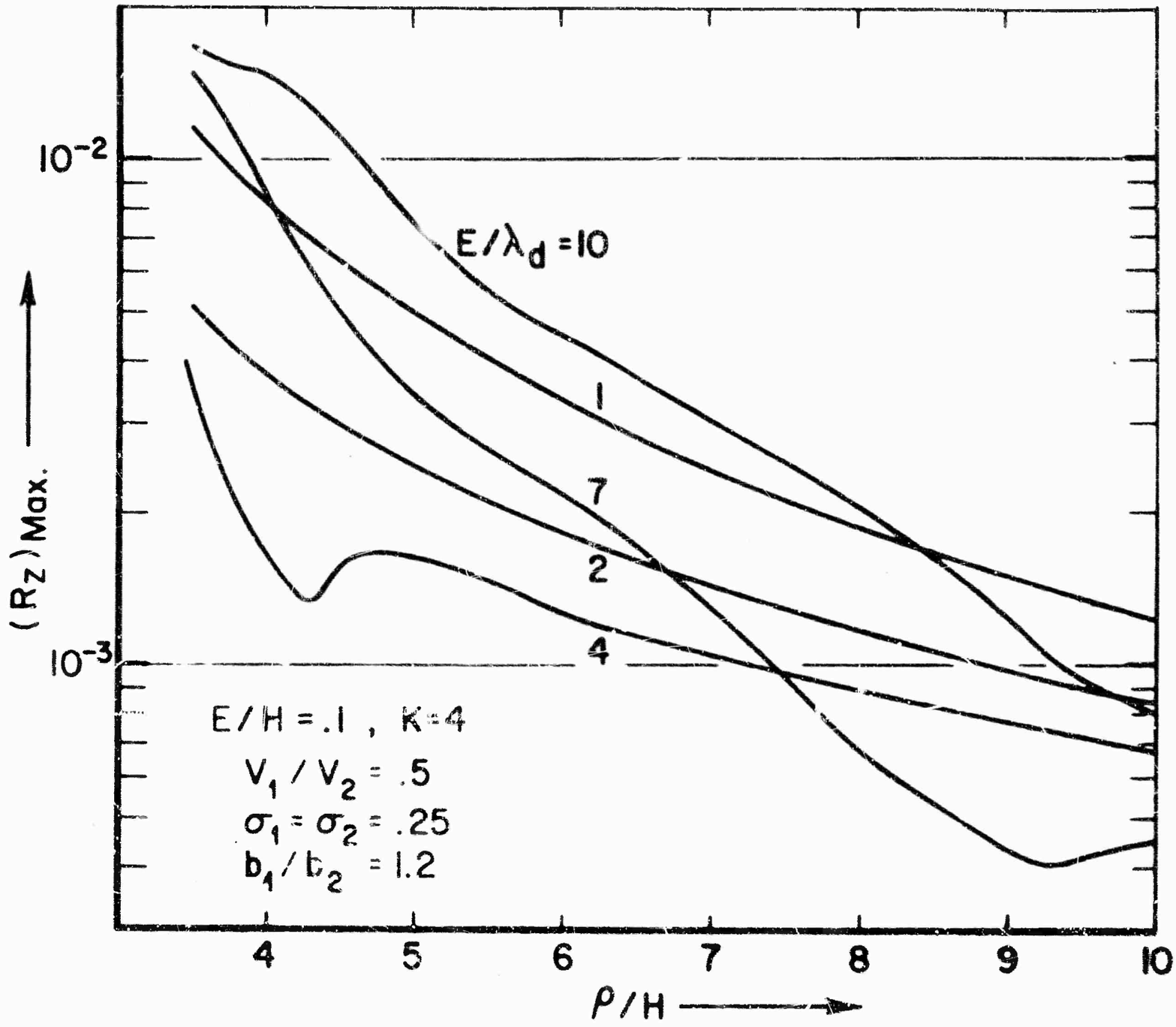

FIGURE 20

LE 44-443